



This is a repository copy of *Analysis and optimal design of a vibration isolation system combined with electromagnetic energy harvester*.

White Rose Research Online URL for this paper:  
<https://eprints.whiterose.ac.uk/150651/>

Version: Accepted Version

---

**Article:**

Diala, U., Mofidian, S.M.M., Lang, Z.-Q. et al. (1 more author) (2019) Analysis and optimal design of a vibration isolation system combined with electromagnetic energy harvester. *Journal of Intelligent Material Systems and Structures*, 30 (16). pp. 2382-2395. ISSN 1045-389X

<https://doi.org/10.1177/1045389x19862377>

---

Diala, U., Mofidian, S. M., Lang, Z.-Q., & Bardaweel, H. (2019). Analysis and optimal design of a vibration isolation system combined with electromagnetic energy harvester. *Journal of Intelligent Material Systems and Structures*, 30(16), 2382–2395. © 2019 The Authors. See: <https://doi.org/10.1177/1045389X19862377>. Article available under the terms of the CC-BY-NC-ND licence (<https://creativecommons.org/licenses/by-nc-nd/4.0/>).

**Reuse**

This article is distributed under the terms of the Creative Commons Attribution-NonCommercial-NoDerivs (CC BY-NC-ND) licence. This licence only allows you to download this work and share it with others as long as you credit the authors, but you can't change the article in any way or use it commercially. More information and the full terms of the licence here: <https://creativecommons.org/licenses/>

**Takedown**

If you consider content in White Rose Research Online to be in breach of UK law, please notify us by emailing [eprints@whiterose.ac.uk](mailto:eprints@whiterose.ac.uk) including the URL of the record and the reason for the withdrawal request.



[eprints@whiterose.ac.uk](mailto:eprints@whiterose.ac.uk)  
<https://eprints.whiterose.ac.uk/>

## Analysis and Optimal Design of a Vibration Isolation System Combined with Electromagnetic Energy Harvester

|                               |  |
|-------------------------------|--|
| Journal:                      | <i>Journal of Intelligent Material Systems and Structures</i>  |
| Manuscript ID                 | JIM-19-009.R1  |
| Manuscript Types:             | Original Article   |
| Date Submitted by the Author: | n/a  |
| Complete List of Authors:     | Diala, Uchenna ; University of Sheffield, Department of Automatic Control and Systems Engineering<br>Mofidian, S M Mahdi ; Louisiana Tech University, Institute for Micromanufacturing<br>Lang, Z Q; University of Sheffield, Automatic Control and Systems Engineering<br>Bardaweel, Hamzeh; Louisiana Tech University, Institute for Micromanufacturing  |
| Keyword:                      | Vibration isolation, Energy Harvesting, vibration isolation energy harvesting, system optimization   |
| Abstract:                     | This work investigates a vibration isolation energy harvesting (VI-EH) system and studies its design to achieve an optimal performance. The system uses a combination of elastic and magnetic components to facilitate its dual functionality. A prototype of the VI-EH device is fabricated and examined experimentally. A mathematical model is developed using first principle and analyzed using Output Frequency Response Function (OFRF). Results from model analysis show an excellent agreement with experiment. Since the VI-EH systems are required to perform two functions simultaneously optimization of the system is carried out to maximize energy conversion efficiency without jeopardizing the system's vibration isolation performance. To the knowledge of the authors, this work is the first effort to tackle the issue of simultaneous vibration isolation energy harvesting using an analytical approach. Explicit analytical relationships describing VI-EH system transmissibility and energy conversion efficiency are developed. Results exhibit a maximum attainable energy conversion efficiency in the order of 1%. Results suggest that for low acceleration levels, lower damping values are favorable and yield higher conversion efficiencies and improved vibration isolation. At higher acceleration, there is a trade-off where lower damping values worsen vibration isolation but yield higher conversion efficiencies. |

1  
2  
3  
4  
5  
6  
7  
8  
9  
10  
11  
12  
13  
14  
15  
16  
17  
18  
19  
20  
21  
22  
23  
24  
25  
26  
27  
28  
29  
30  
31  
32  
33  
34  
35  
36  
37  
38  
39  
40  
41  
42  
43  
44  
45  
46  
47  
48  
49  
50  
51  
52  
53  
54  
55  
56  
57  
58  
59  
60



# **Analysis and Optimal Design of a Vibration Isolation System Combined with Electromagnetic Energy Harvester**

**Uchenna Diala<sup>1</sup>, S.M. Mahdi Mofidian<sup>2</sup>, Zi-Qiang Lang<sup>1</sup> and Hamzeh Bardaweel<sup>2, 3, 4, \*</sup>**

<sup>1</sup> Department of Automatic Control and Systems Engineering, University of Sheffield, UK.

<sup>2</sup> Institute for Micromanufacturing, Louisiana Tech University, Ruston, LA 71272, United States of America.

<sup>3</sup> Department of Mechanical Engineering, Louisiana Tech University, Ruston, LA 71272, United States of America.

<sup>4</sup> Department of Nanosystems Engineering, Louisiana Tech University, Ruston, LA 71272, United States of America.

\* Corresponding author: [hamzehb@latech.edu](mailto:hamzehb@latech.edu)

## Analysis and Optimal Design of a Vibration Isolation System Combined with Electromagnetic Energy Harvester

### Abstract

This work investigates a vibration isolation energy harvesting (VI-EH) system and studies its design to achieve an optimal performance. The system uses a combination of elastic and magnetic components to facilitate its dual functionality. A prototype of the VI-EH device is fabricated and examined experimentally. A mathematical model is developed using first principle and analyzed using Output Frequency Response Function (OFRF). Results from model analysis show an excellent agreement with experiment. Since the VI-EH systems are required to perform two functions simultaneously optimization of the system is carried out to maximize energy conversion efficiency without jeopardizing the system's vibration isolation performance. To the knowledge of the authors, this work is the first effort to tackle the issue of simultaneous vibration isolation energy harvesting using an analytical approach. Explicit analytical relationships describing VI-EH system transmissibility and energy conversion efficiency are developed. Results exhibit a maximum attainable energy conversion efficiency in the order of 1%. Results suggest that for low acceleration levels, lower damping values are favorable and yield higher conversion efficiencies and improved vibration isolation. At higher acceleration, there is a trade-off where lower damping values worsen vibration isolation but yield higher conversion efficiencies.

**Keywords:** Vibration isolation, energy harvesting, system optimization.

# **Analysis and Optimal Design of a Vibration Isolation System Combined with Electromagnetic Energy Harvester**

## **1- Introduction**

Lately, there has been growing interest in developing dual function systems that are capable of both vibration isolation and energy harvesting (Tang and Zuo, 2012; Ali and Adhikari, 2013; Gonzalez-Buelga et al., 2014; Davis and McDowell, 2017; Li et al., 2017; Hu et al., 2017; Chen et al., 2014; Kwon and Oh, 2016; Shen et al., 2018a; Mofidian and Bardaweel, 2019; Yuan et al., 2018). This interest is driven by the continuous improvement in electronics manufacturing which led to deployment of onboard low-power sensors and gadgets (Patel et al., 2012; Knight et al., 2008; Seah et al., 2009; Nammari et al., 2018; Nammari et al., 2017). For instance, onboard sensing units are currently installed on equipment and structures, such as highway bridges and moving vehicles, to monitor their health conditions including temperature, pressure, stress, strain, and humidity (Sazonov et al., 2009; Park et al., 2008; Priya and Inman, 2009; Seah et al., 2009). Undesired vibrations in form of continuous and semi-continuous oscillations are also present in these structures as a result of their dynamic interaction and engagement with the surroundings. While it is desirable to isolate these vibrations and prevent them from traveling through the structure, nonetheless, these oscillations represent free form of kinetic energy. Thus, creating dual function systems that are capable of isolating undesired vibrations while simultaneously converting some of the kinetic energy contained in these oscillations into electric power has been sought (Tang and Zuo, 2012; Ali and Adhikari, 2013; Gonzalez-Buelga et al., 2014; Davis and McDowell, 2017; Li et al., 2017; Hu et al., 2017; Chen et al., 2014; Kwon and Oh, 2016; Shen et al., 2018a; Mofidian and Bardaweel, 2019).

## **Analysis and Optimal Design of a Vibration Isolation System Combined with Electromagnetic Energy Harvester**

Li et al. developed a mechanical metamaterial dual function system comprising a square array of free-standing piezoelectric cantilevers to simultaneously harvest energy and isolate undesired vibrations (Li et al., 2017). Hu et al. presented an analytical model of a vibration isolation energy harvesting acoustic-elastic metamaterial structure (Hu et al., 2017). The proposed structure exhibited a stop band gap for wave transmission while simultaneously achieving energy harvesting by integrating the metamaterial with piezoelectric energy-harvesting element. Davis and McDowell proposed a passive vibration isolation device that harvests energy using post-buckled beam and piezoelectric elements (Davis and McDowell, 2017). Approximately, 0.36  $\mu\text{W}$  electric power was harvested at 2% transmissibility. Li et al. proposed an energy harvesting shock damper system to attenuate vibrations transferred from vehicle-road interaction while simultaneously generating power using a unidirectional rotational mechanism using a mechanical motion rectifier rather than an electrical rectifier to generate DC current (Li et al., 2012). Similarly, Ali and Adhikari studied, theoretically, the performance of a vibration absorber device supplemented with a piezoelectric stack for power recovery (Ali and Adhikari, 2013). In Ref. (Madhav and Ali, 2016) the feasibility of integrating vibration absorber with piezoelectric stack for power generation under random excitations was investigated using probabilistic linear random vibration theory. Results from this theoretical study showed that the recovered power increases with the increase in the mass of structure. Moreover, a device was developed to isolate micro vibrations and harvest energy from micro-jitters for space applications (Kwon and Oh, 2016). The vibration isolation energy harvesting device was able to isolate the desired mass and recovered 5.84  $\mu\text{W}$ . Also, a semi-active energy harvesting

## **Analysis and Optimal Design of a Vibration Isolation System Combined with Electromagnetic Energy Harvester**

vibration suppression system using piezoelectric platform was proposed (Makihara et al., 2007). Additionally, a VI-EH system was developed using a combination of magnetic and mechanical springs (Mofidian and Bardaweel, 2019). While the study was focused on fabrication and proof-of-concept experiments results showed that the fabricated device was able to attenuate oscillations higher than 12.5 [Hz] and recover 0.115 [mW] at 9.81 m.s<sup>-2</sup>.

The work presented in this article uses theoretical models and experiments to analyze a unique VI-EH system and studies the system optimal design to achieve maximum performance. This work is driven by the growing interest and the rising need for VI-EH systems. Therefore, the main focus is to study how to carry out the optimum VI-EH system design. This is needed since VI-EH systems are required to perform two functions simultaneously: Vibration isolation (primary function) and energy harvesting (secondary function). Thus, optimization of the system is a mandate to ensure that maximum amount of energy contained in these oscillations is recovered without jeopardizing the ability of the system to prevent these oscillations from traveling through the structure and causing serious damage (Shen et al., 2018b). To the knowledge of the authors, this work is the first effort to tackle the issue of simultaneous vibration isolation energy harvesting using an analytical approach. By exploiting the OFRF, an approach for the frequency analysis of nonlinear systems, this work provides an explicit analytical relationship between the design objectives (primary and second functions of the VI-EH system) and system design parameters. This can significantly facilitate the VI-EH system's optimal design. Recovered energy (secondary function) had been measured for different VI-EH systems described in literature (For example, 0.36 [μW],

## **Analysis and Optimal Design of a Vibration Isolation System Combined with Electromagnetic Energy Harvester**

5.84 [ $\mu\text{W}$ ], and 0.115 [ $\text{mW}$ ] in (Davis and McDowell, 2017), (Kwon and Oh, 2016), and (Mofidian and Bardaweel, 2019), respectively). However, these articles did not report any details about the vibration isolation effectiveness and power conversion efficiency of the dual function systems. The work presented here formulates transparent performance metrics by developing explicit analytical relationship between all design objectives and system parameters. This is expected to be able to fundamentally resolve the problem of how to simultaneously address vibration isolation and energy harvesting requirements for a VI-EH system.

Description of the VI-EH device and basic measurements are presented in **Section. 2**. The model formulation and OFRF representation are described in **Section. 3**. System design, optimization process, and analysis are presented in **Section. 4**. Conclusions are reached in **Section. 5**.

## **2- Experiment**

This section describes the hardware design of the VI-EH device adopted in this work, fabrication, and experimental work carried out to characterize the device and obtain necessary parameters that are needed to perform an optimal design for the VI-EH system.

### **2.1 VI-EH Device: Hardware Design and Fabrication**

Figure 1 (a-c) shows the VI-EH device fabricated and adopted in this work. A group of magnets, an elastic planar mechanical spring, coils, and air holes constitute the major components of the adopted VI-EH device. The three magnets are arranged in a repulsive configuration causing the solid magnet to float between the top and bottom fixed ring magnets. The mechanical spring guides the movement of the levitated

## **Analysis and Optimal Design of a Vibration Isolation System Combined with Electromagnetic Energy Harvester**

magnet and prevents it from realigning itself with the top and bottom fixed ring magnets. A rod is used to connect the mechanical and magnetic springs to the isolated mass as shown in Figure 1.

External disturbance of the system causes the levitated magnet to move vertically. Viscous damping is then the result of air being pushed through the air holes. Energy harvesting is achieved using stationary coils fixed around the rest position of the levitated magnet. As the levitated magnet moves, voltage is induced in the coil. Thus, the kinetic energy from the oscillations is converted into electric energy. The coils not only serve as a mechanism for power extraction but also introduce additional damping force as a result of eddy currents induced in the coil because of variation in magnetic flux as the levitated magnet is displaced (Sodano et al., 2005). Thus, the dual-functionality of the device is achieved through a combination of elastic and magnetic springs as well as viscous damping due to airflow, and magnetically-induced damping due to levitated magnet movement inside the coil. The damping (viscous and magnetic) and stiffness (mechanical and magnetic spring) form the platform for vibration isolation. Simultaneously, the levitated magnet movement inside the coil forms the base for converting the kinetic energy of vibrations into electric charge.

This VI-EH design shown in Figure 1 is adopted because it offers unique features that are essential for vibration isolation and energy harvesting. Of these unique features is the use of magnetic components to achieve its dual-functionality. For example, an essential limitation of piezoelectrics is their inherently large internal resistance (Gao et al., 2018). Consequently, large load resistance is required to obtain optimum power transfer. This results in very small output currents that are well below

## **Analysis and Optimal Design of a Vibration Isolation System Combined with Electromagnetic Energy Harvester**

the threshold of currents required to operate onboard sensors, i.e. 10-50 mA (Gao et al., 2018). Unlike electrostatic and piezoelectric-based devices, electromagnetic-type devices have significantly lower output impedance (Rahimi et al., 2012). This results in no further required impedance matching at the output stage and, therefore, simpler circuitry. On the other hand, magnetic field-based devices offer larger energy densities (Zahn, 2001). In addition, electromagnetic energy harvesters do not need external voltage supply necessary for electrostatic energy harvesters. The mass of the magnet itself also reduces the resonant frequency of the device which further enables low frequency specialization (Zorlu et al., 2011). Therefore, the use of electromagnetic based energy harvesting unit, instead of piezoelectric, in the VI-EH design makes it , arguably, most suitable type for real-world applications (Liu et al., 2018; Zhang et al., 2016).

Additive manufacturing was used to fabricate the exterior casing and the mechanical spring using Polylactic acid (PLA) thermoplastic filament and Thermoplastic Poly-Urethane (TPU) rubber-like filament, respectively. Neodymium iron boron (NdFeB) magnets were used to build the magnetic spring. The stationary coil was 40 AWG copper coil positioned around the static position of the levitated magnet. Detailed geometry, dimensions, and design specifications are shown in Figure 1c.

### **2.2- Force measurements and system parameters**

Essential for model development and validation, and device optimization shown in Figure 1, is obtaining system parameters including stiffness and damping characteristics. Figure 2 shows the experiment setup used to estimate restoring forces of both mechanical and magnetic springs. A test stand (SHIMPO FGS-250W),

## Analysis and Optimal Design of a Vibration Isolation System Combined with Electromagnetic Energy Harvester

displacement sensor (KEYENCE IL-100), digital force sensor (SHIMPO FG-3006), data acquisition system (NI myDAQ), power supply, and a PC constitute the experiment setup used to measure restoring forces. Figure 3 shows the total restoring force of both mechanical and magnetic springs measured using the experiment setup shown in Figure 2. The total restoring force was then fit to a third order polynomial of the form  $k_1 z + k_3 z^3$ , where  $z$  is the relative displacement of the VI-EH device, and the respective linear and nonlinear stiffness coefficients,  $k_1$  and  $k_3$  were then extracted. Natural frequency,  $\omega_n$  and total damping,  $c_1$ , of the system were also estimated. This was done by holding the VI-EH device firmly in place, bringing it to a predetermined height, and then releasing it. In this experiment, no external excitation was applied, and therefore, the dual-purpose device acted as damped un-driven oscillator. The logarithmic decrement method was then used to estimate the total damping,  $c_1$ , of the system and natural frequency,  $\omega_n$ . Measured system parameters of the fabricated VI-EH device and its properties are summarized in Table I. These measured values were then used in model validation and system optimization.

### 3- Theory: Model and Analysis

Dynamic Model formulation and performance metrics for the VI-EH system are described in this section. Additionally, the OFRF method is used to analyze the dynamic performances of the VI-EH system. Relative displacement transmissibility, absolute displacement transmissibility, energy conversion efficiency, input power, and output power needed for system optimization are introduced and described using the OFRF concept.

## Analysis and Optimal Design of a Vibration Isolation System Combined with Electromagnetic Energy Harvester

### 3.1 Model Formulation

Figure 4 shows model schematic of the VI-EH device. The system represents a single-degree-of-freedom (SDOF) with mass,  $m$  connected to a linear damper of damping coefficient  $c_1$  and nonlinear spring characterized by linear,  $k_1$  and nonlinear,  $k_3$  stiffness coefficients, respectively. It is assumed that lateral vibrations are absent and, therefore, the effective mass,  $m$  is displaced vertically in response to ground excitation,  $y(t)$ . Therefore, the equation of motion of the moving mass is given by:

$$m\ddot{z} + c_1\dot{z} + k_1z + k_3z^3 = -m\ddot{y} \quad (1)$$

where  $z = x - y$ , and  $c_1 = c_e + c_m$  is the total magnetic and mechanical damping in the system, i.e.  $c_e$  and  $c_m$  respectively. For a ground harmonic excitation input, i.e.  $y = Y\sin(\omega t)$ , where  $\omega$  and  $Y$  are the excitation frequency and amplitude of the ground excitation input respectively. Therefore, Eq. (1) becomes

$$m\ddot{z} + c_1\dot{z} + k_1z + k_3z^3 = m\omega^2 Y\sin(\omega t) \quad (2)$$

Absolute displacement transmissibility,  $T_a$  and energy conversion efficiency,  $\eta_e$  are the two main performance metrics sought in this work. Displacement transmissibility is a measure of the effectiveness of vibration isolation and relates the amount of oscillations transmitted from the source of excitation to the isolated mass, i.e.  $T_a = \left| \frac{Z+Y}{Y} \right|$ . The average amount of mechanical power input to the VI-EH system from ground harmonic excitation is given as (Wang et al., 2013; Palagummi et al., 2015; Palagummi and Yuan, 2015; Palagummi and Yuan, 2016):

$$P_{in} = \frac{1}{\pi} m Y^2 \omega^3. \quad (3)$$

## Analysis and Optimal Design of a Vibration Isolation System Combined with Electromagnetic Energy Harvester

For the electromagnetic transduction unit shown in Figure 1, coil resistance,  $R_C$  is responsible for energy harvesting in the VI-EH system, the average output (harvested) power across a load resistance,  $R_L$  is given by

$$P_{out} = \frac{1}{2} \cdot \left[ \frac{k_t \omega Z}{R_C + R_L} \right]^2 \cdot R_L \quad (4)$$

where  $k_t = BNI$  and,  $l$  is the length of the coil per turn,  $N$  is the number of coil turns, and  $B$  is the average magnetic flux density in the air gap between the moving magnet mass and the coil. Considering the average output power,  $P_{out}$ , produced by the VI-EH system when subject to ground harmonic excitation with average input mechanical power of  $P_{in}$ , the energy conversion efficiency  $\eta_e$  of the VI-EH system is, then, given by

$$\eta_e(\%) = \frac{P_{out}}{P_{in}} \times 100 \quad (5)$$

In order to achieve an optimal design for the VI-EH system, in next subsection, the OFRF approach will be used to analyze the dynamic model of the VI-EH system given in Eq. (2). The OFRF representation of the relative displacement transmissibility, absolute displacement transmissibility, average output power, and energy conversion efficiency are derived; providing for the first time, analytical expressions for both the displacement transmissibility and energy conversion efficiency of the VI-EH device. These explicit analytical expressions which correlate the design objectives (primary and second functions of the VI-EH system) and design parameters can be used to optimize the performance of the system and maximize its energy conversion efficiency while maintaining vibration isolation characteristics of the device.

## Analysis and Optimal Design of a Vibration Isolation System Combined with Electromagnetic Energy Harvester

### 3.2 Output Frequency Response Function (OFRF)

The dynamic model of the VI-EH system described in Equation (2) is representative of the duffing-equation. Such equation has previously been studied using several mathematical tools including the method of multiple scales (Hu et al., 1998), direct numerical integration (Erturk and Inman, 2011), nonlinear normal forms (Cammarano et al., 2014), and harmonic balance method (Souayah and Kacem, 2014; Mofidian and Bardaweel, 2018). In the current study, the OFRF will be employed for the analysis, design and optimization of the VI-EH system. The advantage of the OFRF is that the method can provide an explicit analytical relationship between the design objective and system parameters. This can significantly facilitate the system design and optimization. An extensive study of the OFRF concept can be found in (Lang et al., 2007; Lang and Billings, 1996; Lang et al., 2013).

Consider the Volterra systems described by the differential equation

$$\sum_{\bar{m}=1}^M \sum_{p=0}^{\bar{m}} \sum_{l_1, \dots, l_{\bar{m}}=0}^L c_{p, \bar{m}-p}(l_1, \dots, l_{\bar{m}}) \prod_{i=1}^p \frac{d^{l_i} z(t)}{dt^{l_i}} \prod_{i=p+1}^{\bar{m}} \frac{d^{l_i} y(t)}{dt^{l_i}} = 0 \quad (6)$$

where  $L$  is the order of the derivative and  $M$  is the maximum degree of nonlinearity in terms of the system input and output,  $y(t)$  and  $z(t)$ , respectively. According to the OFRF method (Lang et al., 2007), the output frequency response of system (6) can be represented by a polynomial function in terms of the system nonlinear characteristic parameters as

$$Z(j\omega) = \sum_{j_1=0}^{m_1} \dots \sum_{j_{S_N}=0}^{m_{S_N}} \phi_{(j_1, \dots, j_{S_N})}(j\omega) \xi_1^{j_1} \dots \xi_{S_N}^{j_{S_N}} \quad (7)$$

## Analysis and Optimal Design of a Vibration Isolation System Combined with Electromagnetic Energy Harvester

where  $m_i$  are the maximum order of  $\xi_i$ ,  $i = 1, \dots, S_N$  in the polynomial expression of the output spectrum,  $Z(j\omega)$  of system (6). Here,  $\phi_{(j_1, \dots, j_{S_N})}(j\omega)$  are complex-valued frequency functions (also called OFRF coefficients) dependent on the system linear parameters and input, where  $j_i = 0, \dots, m_i$  and  $i = 1, \dots, S_N$ . Also,  $\xi_1^{j_1} \dots \xi_{S_N}^{j_{S_N}}$  is a set of monomials (OFRF structure) in terms of the system nonlinear characteristic parameters. Let the set of monomials in the OFRF representation of the  $n$ th-order output spectrum be denoted as  $\mathfrak{M}$  and the frequency function vector be denoted as  $\Phi(j\omega)$ , the OFRF can be described as

$$Z(j\omega) = \mathfrak{M} \cdot \Phi(j\omega)^T \quad (8)$$

where

$$\mathfrak{M} = \bigcup_{n=1}^N M_n \quad (9)$$

Here,  $N$  is the maximum order of nonlinearity taken into account and the monomials,  $M_n$  can be determined using (Lang and Billings, 1996) as

$$M_n = \left[ \bigcup_{l_1, \dots, l_n=0}^L [c_{0,n}(l_1, \dots, l_n)] \right] \cup \left[ \bigcup_{\bar{m}=p=1}^{n-1} \bigcup_{p=1}^{n-(\bar{m}-p)} U_{l_1, \dots, l_n=0}^L ([c_{p,(\bar{m}-p)}(l_1, \dots, l_{\bar{m}})] \otimes M_{n-(\bar{m}-p),p}) \right] \cup \left[ \bigcup_{p=2}^n \bigcup_{l_1, \dots, l_n=0}^L ([c_{p,0}(l_1, \dots, l_{\bar{m}})] \otimes M_{n,p}) \right] \quad (10)$$

where the character ' $\otimes$ ' is the Kronecker product and given by

$$M_{n,p} = \bigcup_{i=1}^{n-p+1} (M_i \otimes M_{n-i,p-1}), M_{n,1} = M_n, M_1 = [1] \quad (11)$$

Then the set of monomials can be obtained as  $\mathfrak{M} = \bigcup_{n=1}^N M_n$

## Analysis and Optimal Design of a Vibration Isolation System Combined with Electromagnetic Energy Harvester

### 3.3 VI-EH System Analysis

In this section, the OFRF method is used in the analytical study of the VI-EH system described by Eq. (2). Dynamic model of the VI-EH system (2) is a special case of Eq. (6) where  $L = 2$  and  $M = 3$  with system parameters obtained as  $c_{10}(2) = m$ ,  $c_{10}(1) = c_1$ ,  $c_{10}(0) = k_1$ ,  $c_{30}(000) = k_3$ ,  $c_{01}(0) = -m\omega^2 Y$ , else  $c_{p,\bar{m}-p} = 0$ . Applying the algorithm for obtaining the OFRF structure (monomials) as presented in Eq. (10) and Eq. (11) to system in Eq. (2) up to 7<sup>th</sup>-order i.e.  $N = 7$ , yields the following monomials in terms of the system's nonlinear parameter  $k_3$

$$\mathfrak{M} = \bigcup_{n=1}^N M_n = [1, k_3, k_3^2, k_3^3, k_3^4, k_3^5, k_3^6, k_3^7] \quad (12)$$

Using the method developed by Lang et al. (Lang et al., 2007) the frequency function vector  $\Phi(j\omega)$  is computed from a training set  $k_3 = [0:0.1:1.4] \times 10^6$  [N.m<sup>-3</sup>] as

$$\Phi(j\omega) = \begin{bmatrix} \phi_0(j\omega) \\ \phi_1(j\omega) \\ \vdots \\ \phi_6(j\omega) \\ \phi_7(j\omega) \end{bmatrix} = (\psi^T \psi)^{-1} \psi^T \cdot \begin{bmatrix} Z(j\omega)|_{k_3(1)} \\ Z(j\omega)|_{k_3(2)} \\ \vdots \\ Z(j\omega)|_{k_3(14)} \\ Z(j\omega)|_{k_3(15)} \end{bmatrix} \quad (13)$$

where

$$\psi = \begin{bmatrix} 1 & k_3(1) & k_3^2(1) & \cdots & k_3^6(1) & k_3^7(1) \\ 1 & k_3(2) & k_3^2(2) & \cdots & k_3^6(2) & k_3^7(2) \\ \vdots & \vdots & \vdots & \ddots & \vdots & \vdots \\ 1 & k_3(15) & k_3^2(15) & \cdots & k_3^6(15) & k_3^7(15) \end{bmatrix} \quad (14)$$

and  $Z(j\omega)|_{k_3(i)}$  represents the output spectrum of the system when  $k_3 = k_3(i) = (i-1) \times 10^6$ .

## Analysis and Optimal Design of a Vibration Isolation System Combined with Electromagnetic Energy Harvester

Therefore, the OFRF of dynamic system in Eq. (2) derived for each (four) excitation level,  $s = 0.25g, 0.5g, 0.75g$  and  $1g$  [ $m/s^2$ ], is given as

$$Z^{(s)}(j\omega, k_3) = \sum_{r=0}^R \phi_r^{(s)}(j\omega) k_3^r \quad \text{where } R = 7 \text{ and } s = 0.25g, 0.5g, 0.75g \text{ and } 1g [m/s^2] \quad (15)$$

where  $\phi_r^{(s)}(j\omega)$  are the frequency functions dependent on the  $s$ th system input level and linear characteristic parameters,  $c_1$  and  $k_1$ . Moreover, the squared magnitudes of the output response of Eq. (15) are described as (Jing et al., 2008)

$$\begin{cases} |Z^{(s)}(j\omega, k_3)|^2 = Z^{(s)}(j\omega, k_3) \cdot Z^{(s)}(-j\omega, k_3) = \left( \sum_{r=0}^R \phi_r^{(s)}(j\omega) k_3^r \right) \left( \sum_{r=0}^R \phi_r^{(s)}(-j\omega) k_3^r \right) \\ = \phi_0^{(s)} \phi_0^{(s)*} + \sum_{t=1}^{\infty} \left( k_3^t \sum_{\tau=0}^t \phi_{\tau}^{(s)} \phi_{t-\tau}^{(s)*} \right) \\ = \delta_0^{(s)} + \delta_1^{(s)} k_3 + \delta_2^{(s)} k_3^2 + \dots + \delta_{13}^{(s)} k_3^{13} + \delta_{14}^{(s)} k_3^{14} \\ = \sum_{r=0}^{\tilde{R}} \delta_r^{(s)}(\omega) k_3^r \quad \text{where } \tilde{R} = 14 \text{ and } s = 0.25g, 0.5g, 0.75g \text{ and } 1g [m/s^2] \end{cases} \quad (16)$$

where  $\delta_r^{(s)}(\omega)$ ,  $r = 0, 1, 2, \dots, \tilde{R}$ , are the OFRF coefficients of the squared magnitude of the output response given in Eq. (16) for  $s$ th system input level, at excitation frequency,  $\omega$ .

Substituting Eq. (16) in Eq. (4) yields

$$\begin{cases} P_{out}^{(s)}(\omega, k_3) = \frac{1}{2R_L} \cdot \left[ \frac{k_t \omega R_L}{R_C + R_L} \right]^2 \cdot |Z^{(s)}|^2 \\ = \frac{1}{2R_L} \cdot \left[ \frac{k_t \omega R_L}{R_C + R_L} \right]^2 \cdot \left[ \sum_{r=0}^{\tilde{R}} \delta_r^{(s)}(\omega) k_3^r \right] \\ = \alpha(\omega) \cdot \left[ \sum_{r=0}^{\tilde{R}} \delta_r^{(s)}(\omega) k_3^r \right] \quad \text{where } \alpha(\omega) = \frac{1}{2R_L} \cdot \left[ \frac{k_t \omega R_L}{R_C + R_L} \right]^2 \end{cases} \quad (17)$$

Similarly, substituting Eq. (3) and Eq. (17) in Eq. (5) yields

## Analysis and Optimal Design of a Vibration Isolation System Combined with Electromagnetic Energy Harvester

$$\left\{ \begin{aligned} \eta_e^{(s)}(\omega, k_3) &= \frac{\frac{1}{2R_L} \cdot \left[ \frac{k_t \omega R_L}{R_C + R_L} \right]^2 \cdot \left[ \sum_{r=0}^{\tilde{R}} \delta_r^{(s)}(\omega) k_3^r \right]}{\frac{1}{\pi} m \omega^3 Y^2} \\ &= \frac{\pi \omega}{2mR_L(\omega^2 Y)^2} \cdot \left[ \frac{k_t \omega R_L}{R_C + R_L} \right]^2 \cdot \left[ \sum_{r=0}^{\tilde{R}} \delta_r^{(s)}(\omega) k_3^r \right] \\ &= \lambda(\omega) \cdot \left[ \sum_{r=0}^{\tilde{R}} \delta_r^{(s)}(\omega) k_3^r \right] \quad \text{where } \lambda(\omega) = \frac{\pi \omega}{2mR_L(\omega^2 Y)^2} \cdot \left[ \frac{k_t \omega R_L}{R_C + R_L} \right]^2 \end{aligned} \right. \quad (18)$$

From Eq. (17) and Eq. (18), the following representations for  $P_{out}$  and  $\eta_e$  can be obtained:

$$\left\{ \begin{aligned} P_{out}^{(s)}(\omega, k_3) &= \sum_{r=0}^{\tilde{R}} \varphi_r^{(s)}(\omega) \cdot k_3^r \quad \left\{ \text{where } \varphi_r^{(s)}(\omega) = \alpha(\omega) \cdot \delta_r^{(s)}(\omega) \right\} \\ \eta_e^{(s)}(\omega, k_3) &= \sum_{r=0}^{\tilde{R}} \beta_r^{(s)}(\omega) k_3^r \quad \left\{ \text{where } \beta_r^{(s)}(\omega) = \lambda(\omega) \cdot \delta_r^{(s)}(\omega) \right\} \end{aligned} \right. \quad (19)$$

Eq. (19) shows the OFRF representation for the average output power,  $P_{out}$  and the energy conversion efficiency,  $\eta_e$  of the VI-EH system in Eq. (2), respectively for each acceleration level,  $s$ . The corresponding OFRF for the absolute displacement transmissibility,  $T_a$ , under excitation  $s$ , is then given as

$$T_a^{(s)}(\omega, k_3) = \sum_{r=0}^{\tilde{R}} \rho_r^{(s)}(\omega) \cdot k_3^r \quad (20)$$

where  $\varphi_r^{(s)}(\omega)$ ,  $\beta_r^{(s)}(\omega)$  and  $\rho_r^{(s)}(\omega)$  are frequency functions dependent on the system input and linear characteristic parameters and  $\omega$  is the driving frequency of interest. It should also be noted that,  $\varphi_r^{(s)}(\omega)$ ,  $\beta_r^{(s)}(\omega)$  and  $\rho_r^{(s)}(\omega)$  are the OFRF coefficients of the average output power,  $P_{out}^{(s)}$ , energy conversion efficiency,  $\eta_e^{(s)}$ , and absolute displacement transmissibility,  $T_a^{(s)}$ , of the VI-EH system, for  $s$ th system input level, at excitation frequency,  $\omega$ . It should be noted that the OFRF representation of the system

## Analysis and Optimal Design of a Vibration Isolation System Combined with Electromagnetic Energy Harvester

performance indices of interest is each unique for one of the four specific input acceleration levels of  $s = 0.25g, 0.5g, 0.75g$  and  $1g$  [ $m/s^2$ ] considered in this work.

A comparison of the OFRF results with that obtained using the Runge-kutta algorithm (ODE45 in MATLAB) over the system parameter values outside the OFRF training range (in this case,  $k_3 = 1.5 \times 10^6 \text{ Nm}^{-3}$ ) is shown in Figure 5(a-c) indicating that the OFRF provides a very good representation for the actual system performance.

### 3.4 Model Validation

In order to validate the developed model both displacement transmissibility,  $T_a$  and energy conversion efficiency,  $\eta_e$  of the VI-EH device were measured simultaneously. The apparatus used for these tests is shown in Figure 6. The experiment setup consisted of a shaker table (VT-500, SENTEK DYNAMICS), power amplifier (LA-800, SENTEK DYNAMICS), vibration controller (S81B-P02, SENTEK DYNAMICS), two accelerometers (PCB333B30 model, PCB Piezotronics), data acquisition system (NI myDAQ), and a PC. The VI-EH device was firmly fixed on the shaker table top and driven at accelerations of  $0.5g$  [ $m/s^2$ ]. The voltage output from the VI-EH device across load resistance,  $R_L$ , and the acceleration level transmitted to the isolated mass were simultaneously measured. Induced voltage was measured across a load resistance using decade box (GLOBAL SPECIALTIES RDB-10) and extracted power,  $P_{out}$  was then estimated.

Measured displacement transmissibility, and power extracted by the VI-EH device are shown in Figures 7 and 8, respectively. Additionally, model predictions are compared to measured data as shown in Figure 7-8. Results reveal good agreement

## Analysis and Optimal Design of a Vibration Isolation System Combined with Electromagnetic Energy Harvester

between experimental data and model simulations. Figure 7 demonstrates that transmissibility of the VI-EH device drops to less than unity, i.e.  $T_a < 1$  at corresponding non-dimensional frequency,  $\Omega = \frac{\omega}{\omega_n} = 1.42$  when loading level is 0.5g [m s<sup>-2</sup>]. The ability of the device to extract electric power from the ground excitation during the dynamic operation is also evident in Figure 8. The power extracted during the dynamic operation of the VI-EH device was measured across a load resistance,  $R_L = 1280$  [ohms]. The power produced by the device when transmissibility dropped to unity, i.e.  $T_a = 1$  was approximately 0.34 [mW] at 0.5g [m/s<sup>2</sup>]. This demonstrates the ability of the device to simultaneously isolate the mass and scavenge kinetic energy from these oscillations. Optimization process of the VI-EH system is discussed next.

### 4 System Design and Optimization

A simulation study of the performance of the VI-EH system subject to variation in linear damping,  $c_1$  around the experimentally measured value of  $c_1 = 2.7$  [N s m<sup>-1</sup>] while keeping  $k_3$  fixed as  $1.368 \times 10^6$  [N m<sup>-3</sup>] is shown in Figure 9(a-c). In designing the VI-EH system over the isolation region ( $\omega > \omega_n\sqrt{2}$ ), it is apparent, as presented in Figure 9a that at low levels of acceleration, i.e. 0.25g and 0.5g, transmissibility,  $T_a$ , increased slightly as the linear damping  $c_1$  increased. On the other hand, at higher level of acceleration (0.75g and 1.0g), an increase in linear damping,  $c_1$  leads to decrease in transmissibility values. This becomes an important feature of the nonlinear VI-EH system in comparison to a linear system. That is, an inherent limitation of typical linear isolation systems ( $k_3 = 0$ ) is that its absolute displacement transmissibility increases as linear damping is increased for all acceleration levels. Figure 9b suggests that, for fixed

## Analysis and Optimal Design of a Vibration Isolation System Combined with Electromagnetic Energy Harvester

acceleration level, the average output power decreases at higher linear damping. Nonetheless, as the linear damping,  $c_1$  increases the rate of decay in output power  $P_{out}$  is larger at higher levels of excitations. It also reveals that, for fixed damping, the average output power increases as the excitation level increases. Nonetheless, a closer inspection of Figure 9c shows that while the energy conversion efficiency,  $\eta_e$ , is sensitive to linear damping,  $c_1$ , it is independent of the excitation level. This is possibly due to the fact that an increase in input mechanical power at higher acceleration is accompanied by increase in the output power. Overall, for low acceleration levels, lower damping values are favorable and yield higher energy conversion efficiencies (Figure 9c) and improved vibration isolation (Figure 9a.) At higher acceleration levels, there is a trade-off where lower damping values worsen vibration isolation characteristics of the VI-EH system (Figure 9a) but yield higher energy conversion efficiencies (Figure 9c).

Next, the linear damping parameters are, first, designed under low base-excitation and, then, used to design and optimize the nonlinear stiffness  $k_3$  at different excitation levels using the OFRF approach. Using the measured natural frequency,  $\omega_n = 55.6$  [rad/s] and design criteria for the system, i.e.

$$T_a = 0.9855 \text{ when } \omega = \omega_n \sqrt{2}, \text{ or } \Omega = \frac{\omega}{\omega_n} = 1.42$$

$k_1$  and  $c_1$  are obtained as:

## Analysis and Optimal Design of a Vibration Isolation System Combined with Electromagnetic Energy Harvester

$$\begin{cases} k_1 = m\omega_n^2 \\ c_1 = 2\xi m\omega_n \\ \text{where } \xi \text{ is determined from equation} \\ T_a = \sqrt{\frac{1 + (2\xi\Omega)^2}{(1 - \Omega^2)^2 + (2\xi\Omega)^2}} \end{cases} \quad (21)$$

Using the system linear parameters  $k_1$  and  $c_1$ , thus determined, the OFRF in terms of the nonlinear parameter  $k_3$  is employed for the design and optimization of the VI-EH system as follows.

From the OFRF representation for the energy conversion efficiency and the absolute displacement transmissibility obtained in Section 3, the optimization problem for nonlinear parameter  $k_3$  can be formulated as;

$$\begin{aligned} & \max_{k_3} \eta_e^s(\omega, k_3) \\ & \text{subject to} \begin{cases} k_3 - 1.4 \times 10^6 \leq 0 \\ \sum_{r=0}^R \rho_r^s(\omega) \cdot k_3^r - 1 < 0 \end{cases} \end{aligned} \quad (22)$$

where  $\omega = \omega_n\sqrt{2} = 79$  [rad/s], which is essential constraint for vibration isolation characteristics of the VI-EH system (primary function). The solution to the optimization problem (22) under each of the four levels of ground acceleration inputs of  $s = 0.25g, 0.5g, 0.75g$  and  $1g$  [m/s<sup>2</sup>] is presented in Table II.

From Table II, it is evident that the maximum nonlinear stiffness coefficient  $k_3 = 1.4 \times 10^6$  Nm<sup>-3</sup> results in a maximum conversion efficiency,  $\eta_{e_{\max}}$  at the first three levels of acceleration, that is,  $0.25g, 0.5g$  and  $0.75g$  [ms<sup>-2</sup>], respectively. Nonetheless, at acceleration level of  $1.0g$  [ms<sup>-2</sup>], increasing the nonlinear stiffness coefficient,  $k_3$  beyond  $0.8 \times 10^6$  [N m<sup>-3</sup>] causes the transmissibility to grow beyond unity, which violates the second constraint of design. Therefore, the optimal solution is  $k_3 = 0.8 \times 10^6$  Nm<sup>-3</sup>.

## Analysis and Optimal Design of a Vibration Isolation System Combined with Electromagnetic Energy Harvester

Overall, the maximum energy conversion efficiency of the VI-EH system is less than 1%, which is relatively low. This is because the primary function (vibration isolation) of the VI-EH system is to maintain transmissibility to be less than unity, i.e.  $T_a < 1$ . However, it is worth pointing out that even though the conversion efficiency is low, converting some of the free and abundant kinetic energy using a stack of VI-EH devices could still be useful for onboard low-power sensors and gadgets.

The above optimization problem (22) was solved for each of the four input levels. If a design needs to take into account all the four input levels, a weighted sum of the objective functions associated with each input level such that

$$\begin{cases} T_a^K = \kappa_1 \cdot T_a^{(0.25g)} + \kappa_2 \cdot T_a^{(0.5g)} + \kappa_3 \cdot T_a^{(0.75g)} + \kappa_4 \cdot T_a^{(1g)} \\ P_{out}^K = \kappa_1 \cdot P_{out}^{(0.25g)} + \kappa_2 \cdot P_{out}^{(0.5g)} + \kappa_3 \cdot P_{out}^{(0.75g)} + \kappa_4 \cdot P_{out}^{(1g)} \\ \eta_e^K = \kappa_1 \cdot \eta_e^{(0.25g)} + \kappa_2 \cdot \eta_e^{(0.5g)} + \kappa_3 \cdot \eta_e^{(0.75g)} + \kappa_4 \cdot \eta_e^{(1g)} \end{cases} \quad (23)$$

where  $\kappa_1 + \kappa_2 + \kappa_3 + \kappa_4 = 1$  can be used. Eq (23) can be further written as

$$\begin{cases} T_a^K = \sum_{r=0}^{\tilde{R}} [\kappa_1 \rho_r^{(0.25g)}(\omega) + \kappa_2 \rho_r^{(0.5g)}(\omega) + \kappa_3 \rho_r^{(0.75g)}(\omega) + \kappa_4 \rho_r^{(1g)}(\omega)] \cdot k_3^r \\ P_{out}^K = \sum_{r=0}^{\tilde{R}} [\kappa_1 \varphi_r^{(0.25g)}(\omega) + \kappa_2 \varphi_r^{(0.5g)}(\omega) + \kappa_3 \varphi_r^{(0.75g)}(\omega) + \kappa_4 \varphi_r^{(1g)}(\omega)] \cdot k_3^r \\ \eta_e^K = \sum_{r=0}^{\tilde{R}} [\kappa_1 \beta_r^{(0.25g)}(\omega) + \kappa_2 \beta_r^{(0.5g)}(\omega) + \kappa_3 \beta_r^{(0.75g)}(\omega) + \kappa_4 \beta_r^{(1g)}(\omega)] \cdot k_3^r \end{cases} \quad (24)$$

Consider, for example, the conversion efficiency as the design objective. Then, the optimization of the VI-EH system taking into account all four loading conditions into account can be formulated as

$$\begin{aligned} & \max_{k_3} \quad \eta_e^K \\ & \text{s.t.} \quad \begin{cases} k_3 - 1.4 \times 10^6 \leq 0 \\ \sum_{r=0}^{\tilde{R}} [\kappa_1 \rho_r^{(0.25g)}(\omega) + \kappa_2 \rho_r^{(0.5g)}(\omega) + \kappa_3 \rho_r^{(0.75g)}(\omega) + \kappa_4 \rho_r^{(1g)}(\omega)] \cdot k_3^r - 1 < 0 \end{cases} \end{aligned} \quad (25)$$

where  $\omega = \omega_n \sqrt{2} = 79$  [rad/s].

## Analysis and Optimal Design of a Vibration Isolation System Combined with Electromagnetic Energy Harvester

The solutions to the optimization problem (25) under the following three choices of weights

$$\kappa_1 = \kappa_2 = \kappa_3 = \kappa_4 = 0.25$$

$$\kappa_1 = \kappa_2 = 0.5, \kappa_3 = \kappa_4 = 0$$

and

$$\kappa_1 = \kappa_2 = 0, \kappa_3 = \kappa_4 = 0.5$$

are shown in Table III. The results indicate that the conversion efficiency is almost the same in all the cases. However, in the case of  $\kappa_1 = \kappa_2 = 0.5, \kappa_3 = \kappa_4 = 0$ , where two lowest input levels are considered for the optimal design, the average power output is the lowest. In the case of  $\kappa_1 = \kappa_2 = \kappa_3 = \kappa_4 = 0.25$  where all the four loading levels are considered, the average power output become larger. In the case of  $\kappa_1 = \kappa_2 = 0, \kappa_3 = \kappa_4 = 0.5$  where the two largest input levels are considered, the average power output is the highest.

The optimal designs introduced above were conducted based on an OFRF representation of the transmissibility, conversion efficiency, and output power of the VI-EH system in terms of the system's nonlinear stiffness coefficient,  $k_3$ . The advantage of this design approach over other techniques is that an explicit relationship between the design objective and design parameter is exploited to find an optimal solution to the design. Fig 10 shows these OFRF representations.

In Figure 10a, the effect of  $k_3$  on transmissibility  $T_a$  is evident. For a fixed acceleration, an increase in  $k_3$  yields higher transmissibility,  $T_a$  (Figure 10a) and higher efficiency (Figure 10c). Also, the rates of increase in transmissibility  $T_a$  and efficiency,  $\eta_e$ , become larger (steeper) as the acceleration level is increased. This is primarily due

## Analysis and Optimal Design of a Vibration Isolation System Combined with Electromagnetic Energy Harvester

to the stiffness hardening nonlinearity effects which manifest itself at higher accelerations. It is worth mentioning that for the case of linear stiffness ( $k_3 = 0$ ), the VI-EH transmissibility,  $T_a$  is independent of the excitation level as depicted in Figure 10a. On the other hand, Figure 10b suggests that, at all excitation levels, the output power,  $P_{out}$  is insensitive to nonlinear stiffness coefficient,  $k_3$ . However, Figure 10b shows that the output power,  $P_{out}$ , is very sensitive to the excitation level, making significant improvement in harvested power when increasing the excitation level. Overall, Figure 10 reveals that for fixed acceleration level, increasing the nonlinear stiffness coefficient,  $k_3$ , results in higher conversion efficiencies (Figure 10c) but worsens the vibration isolation of the VI-EH system, transmitting more vibration to the isolated mass (Figure 10a). These observations further confirm the validity of the optimal solutions that have been obtained above by solving optimization problems (22) and (25), respectively, and demonstrate that the OFRF based optimization has good potential to be applied for the optimal design of the VI-EH systems in practice.

## 5 Conclusions

Driven by the growing interest in simultaneous vibration isolation and energy harvesting this work was focused on investigating optimal design of dual function VI-EH systems. The adopted VI-EH system uses a combination of elastic and magnetic components to facilitate its dual functionality, i.e. Vibration isolation (primary function) and energy harvesting (secondary function). A prototype of the VI-EH device was fabricated and used for model validation and design optimization. A mathematical model of the VI-EH system has been developed and analyzed using a nonlinear system

## **Analysis and Optimal Design of a Vibration Isolation System Combined with Electromagnetic Energy Harvester**

frequency analysis approach known as Output Frequency Response Function (OFRF). Explicit analytical relationships between the design objectives (primary and second functions of the VI-EH system) and system design parameters, were developed. To the knowledge of the authors, this work is the first effort to tackle the issue of simultaneous vibration isolation energy harvesting using an analytical approach. Results have shown that the maximum attainable energy conversion efficiency of the VI-EH system was in the order of 1%. Nonetheless, since the primary function (vibration isolation) of the VI-EH system was achieved, harvesting some of the free and abundant kinetic energy contained in these oscillations (secondary function) could be useful in the future as power requirements for onboard sensors is continuously dropping. Other design improvements may lead to improved power metrics. For example, future work will focus on investigating VI-EH systems with nonlinear damping element as well as softening stiffness nonlinearities as possible route to improve performance metrics of the VI-EH system.

### **Reference**

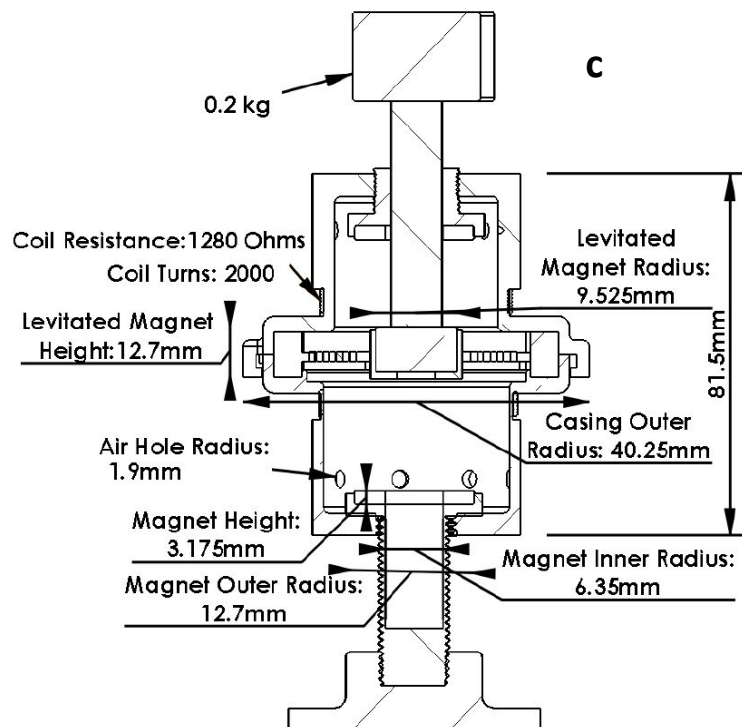
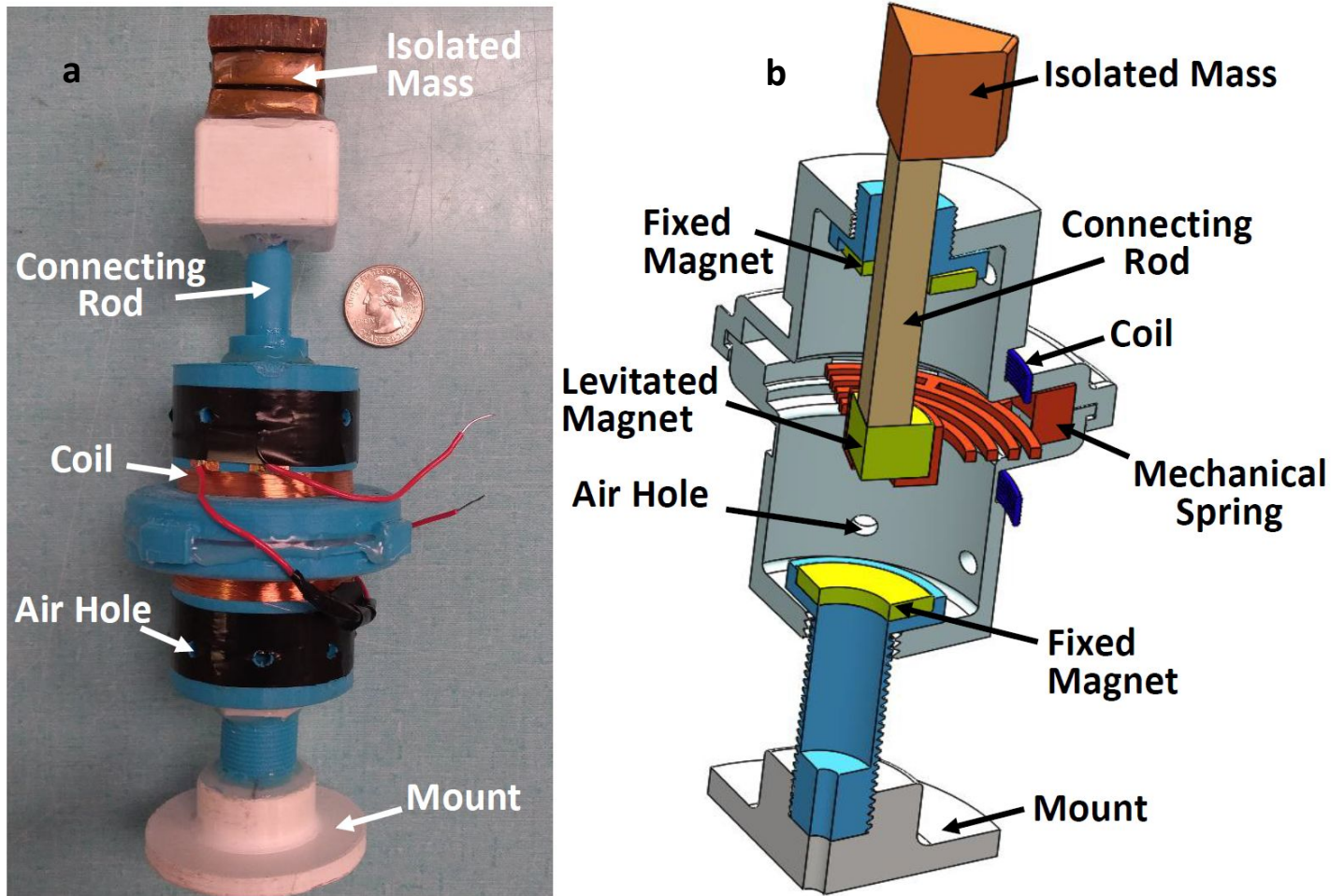
- Ali SF and Adhikari S. (2013) Energy harvesting dynamic vibration absorbers. *Journal of Applied Mechanics* 80: 041004.
- Cammarano A, Neild S, Burrow S, et al. (2014) Optimum resistive loads for vibration-based electromagnetic energy harvesters with a stiffening nonlinearity. *Journal of Intelligent Material Systems and Structures* 25: 1757-1770.
- Chen Z, Guo B, Yang Y, et al. (2014) Metamaterials-based enhanced energy harvesting: A review. *Physica B: Condensed Matter* 438: 1-8.
- Davis R and McDowell M. (2017) Combined Euler column vibration isolation and energy harvesting. *Smart Materials and Structures* 26: 055001.
- Erturk A and Inman D. (2011) Broadband piezoelectric power generation on high-energy orbits of the bistable Duffing oscillator with electromechanical coupling. *Journal of Sound and Vibration* 330: 2339-2353.
- Gao M, Wang Y, Wang Y, et al. (2018) Experimental investigation of non-linear multi-stable electromagnetic-induction energy harvesting mechanism by magnetic levitation oscillation. *Applied Energy* 220: 856-875.

## Analysis and Optimal Design of a Vibration Isolation System Combined with Electromagnetic Energy Harvester

- Gonzalez-Buelga A, Clare L, Cammarano A, et al. (2014) An optimised tuned mass damper/harvester device. *Structural Control and Health Monitoring* 21: 1154-1169.
- Hu G, Tang L, Banerjee A, et al. (2017) Metastructure with piezoelectric element for simultaneous vibration suppression and energy harvesting. *Journal of Vibration and Acoustics* 139: 011012.
- Hu H, Dowell EH and Virgin LN. (1998) Resonances of a harmonically forced Duffing oscillator with time delay state feedback. *Nonlinear Dynamics* 15: 311-327.
- Jing XJ, Lang ZQ and Billings SA. (2008) Output frequency response function-based analysis for nonlinear Volterra systems. *Mechanical systems and signal processing* 22: 102-120.
- Knight C, Davidson J and Behrens S. (2008) Energy options for wireless sensor nodes. *Sensors* 8: 8037-8066.
- Kwon S-C and Oh H-U. (2016) Experimental validation of satellite micro-jitter management strategy in energy harvesting and vibration isolation. *Sensors and Actuators A: Physical* 249: 172-185.
- Lang Z-Q and Billings S. (1996) Output frequency characteristics of nonlinear systems. *International Journal of Control* 64: 1049-1067.
- Lang Z, Guo P and Takewaki I. (2013) Output frequency response function based design of additional nonlinear viscous dampers for vibration control of multi-degree-of-freedom systems. *Journal of Sound and Vibration* 332: 4461-4481.
- Lang ZQ, Billings SA, Yue R, et al. (2007) Output frequency response function of nonlinear Volterra systems. *Automatica* 43: 805-816.
- Li Y, Baker E, Reissman T, et al. (2017) Design of mechanical metamaterials for simultaneous vibration isolation and energy harvesting. *Applied Physics Letters* 111: 251903.
- Li Z, Zuo L, Kuang J, et al. (2012) Energy-harvesting shock absorber with a mechanical motion rectifier. *Smart Materials and Structures* 22: 025008.
- Liu M, Lin R, Zhou S, et al. (2018) Design, simulation and experiment of a novel high efficiency energy harvesting paver. *Applied Energy* 212: 966-975.
- Madhav C and Ali SF. (2016) Harvesting Energy from Vibration Absorber under Random Excitations. *IFAC-PapersOnLine* 49: 807-812.
- Makihara K, Onoda J and Minesugi K. (2007) A self-sensing method for switching vibration suppression with a piezoelectric actuator. *Smart Materials and Structures* 16: 455.
- Mofidian SM and Bardaweel H. (2018) Displacement transmissibility evaluation of vibration isolation system employing nonlinear-damping and nonlinear-stiffness elements. *Journal of Vibration and Control* 24: 4247-4259.
- Mofidian SM and Bardaweel H. (2019) A dual-purpose vibration isolator energy harvester: Experiment and model. *Mechanical Systems and Signal Processing* 118: 360-376.
- Nammari A, Caskey L, Negrete J, et al. (2018) Fabrication and characterization of non-resonant magneto-mechanical low-frequency vibration energy harvester. *Mechanical Systems and Signal Processing* 102: 298-311.
- Nammari A, Doughty S, Savage D, et al. (2017) Design and analysis of a small-scale magnetically levitated energy harvester utilizing oblique mechanical springs. *Microsystem Technologies* 23: 4645-4657.
- Palagummi S and Yuan F-G. (2016) Magnetic levitation and its application for low frequency vibration energy harvesting. *Structural Health Monitoring (SHM) in Aerospace Structures*. Elsevier, 213-251.
- Palagummi S and Yuan F. (2015) An optimal design of a mono-stable vertical diamagnetic levitation based electromagnetic vibration energy harvester. *Journal of Sound and Vibration* 342: 330-345.
- Palagummi S, Zou J and Yuan F. (2015) A horizontal diamagnetic levitation based low frequency vibration energy harvester. *Journal of Vibration and Acoustics* 137: 061004.
- Park G, Rosing T, Todd MD, et al. (2008) Energy harvesting for structural health monitoring sensor networks. *Journal of Infrastructure Systems* 14: 64-79.

## Analysis and Optimal Design of a Vibration Isolation System Combined with Electromagnetic Energy Harvester

- Patel S, Park H, Bonato P, et al. (2012) A review of wearable sensors and systems with application in rehabilitation. *Journal of neuroengineering and rehabilitation* 9: 21.
- Priya S and Inman DJ. (2009) *Energy harvesting technologies*: Springer.
- Rahimi A, Zorlu Ö, Muhtaroglu A, et al. (2012) Fully self-powered electromagnetic energy harvesting system with highly efficient dual rail output. *Sensors Journal, IEEE* 12: 2287-2298.
- Sazonov E, Li H, Curry D, et al. (2009) Self-powered sensors for monitoring of highway bridges. *IEEE Sensors Journal* 9: 1422-1429.
- Seah WK, Eu ZA and Tan H-P. (2009) Wireless sensor networks powered by ambient energy harvesting (WSN-HEAP)-Survey and challenges. *Wireless Communication, Vehicular Technology, Information Theory and Aerospace & Electronic Systems Technology, 2009. Wireless VITAE 2009. 1st International Conference on. Ieee*, 1-5.
- Shen W, Zhu S, Xu YL, et al. (2018a) Energy regenerative tuned mass dampers in high-rise buildings. *Structural Control and Health Monitoring* 25.
- Shen W, Zhu S and Zhu H. (2018b) Unify Energy Harvesting and Vibration Control Functions in Randomly Excited Structures with Electromagnetic Devices. *Journal of Engineering Mechanics* 145: 04018115.
- Sodano HA, Bae J-S, Inman DJ, et al. (2005) Concept and model of eddy current damper for vibration suppression of a beam. *Journal of Sound and Vibration* 288: 1177-1196.
- Souayah S and Kacem N. (2014) Computational models for large amplitude nonlinear vibrations of electrostatically actuated carbon nanotube-based mass sensors. *Sensors and Actuators A: Physical* 208: 10-20.
- Tang X and Zuo L. (2012) Simultaneous energy harvesting and vibration control of structures with tuned mass dampers. *Journal of Intelligent Material Systems and Structures* 23: 2117-2127.
- Wang X, Palagummi S, Liu L, et al. (2013) A magnetically levitated vibration energy harvester. *Smart Materials and Structures* 22: 055016.
- Yuan M, Liu K and Sadhu A. (2018) Simultaneous vibration suppression and energy harvesting with a non-traditional vibration absorber. *Journal of Intelligent Material Systems and Structures* 29: 1748-1763.
- Zahn M. (2001) Magnetic fluid and nanoparticle applications to nanotechnology. *Journal of Nanoparticle Research* 3: 73-78.
- Zhang Z, Zhang X, Chen W, et al. (2016) A high-efficiency energy regenerative shock absorber using supercapacitors for renewable energy applications in range extended electric vehicle. *Applied Energy* 178: 177-188.
- Zorlu Ö, Topal ET and KÜlah H. (2011) A vibration-based electromagnetic energy harvester using mechanical frequency up-conversion method. *Sensors Journal, IEEE* 11: 481-488.



1  
2  
3  
4  
5  
6  
7  
8  
9  
10  
11  
12  
13  
14  
15  
16  
17  
18  
19  
20  
21  
22  
23  
24  
25  
26  
27  
28  
29  
30  
31  
32  
33  
34  
35  
36  
37  
38  
39  
40  
41  
42  
43  
44  
45  
46  
47  
48  
49  
50  
51  
52  
53  
54  
55  
56  
57  
58  
59  
60

**Figure 1:** VI-EH device fabricated this work: a) Fully fabricated and assembled VI-EH device, b) Cross-sectional view of the VI-EH device, and c) 2D sketch of the VI-EH device with detailed geometries and dimensions.

For Peer Review

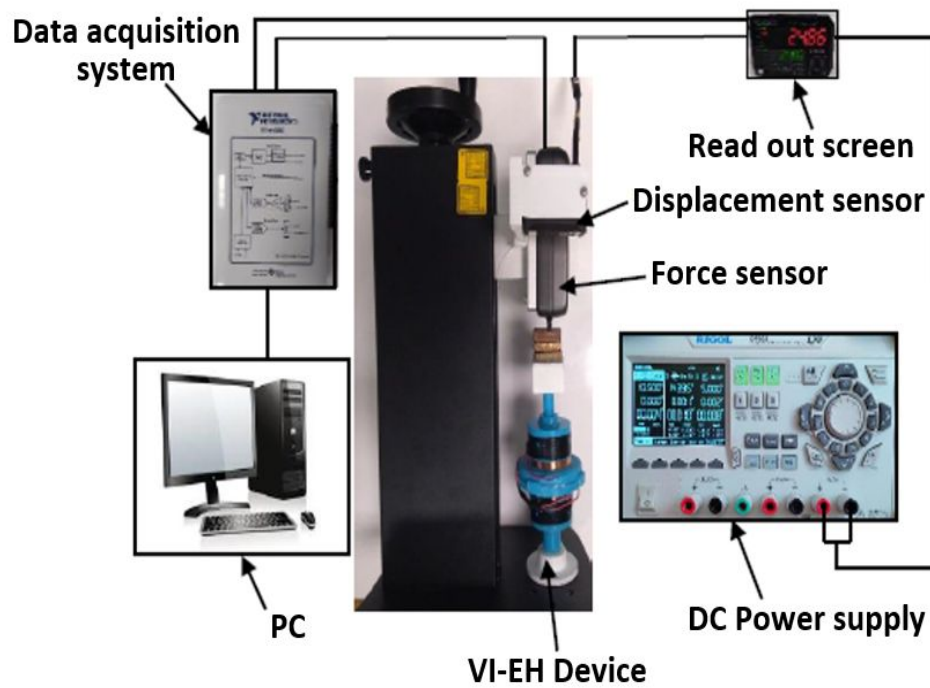


**Figure 2:** Experiment setup used to estimate restoring forces of the VI-EH device.

1  
2  
3  
4  
5  
6  
7  
8  
9  
10  
11  
12  
13  
14  
15  
16  
17  
18  
19  
20  
21  
22  
23  
24  
25  
26  
27  
28  
29  
30  
31  
32  
33  
34  
35  
36  
37  
38  
39  
40  
41  
42  
43  
44  
45  
46  
47  
48  
49  
50  
51  
52  
53  
54  
55  
56  
57  
58  
59  
60

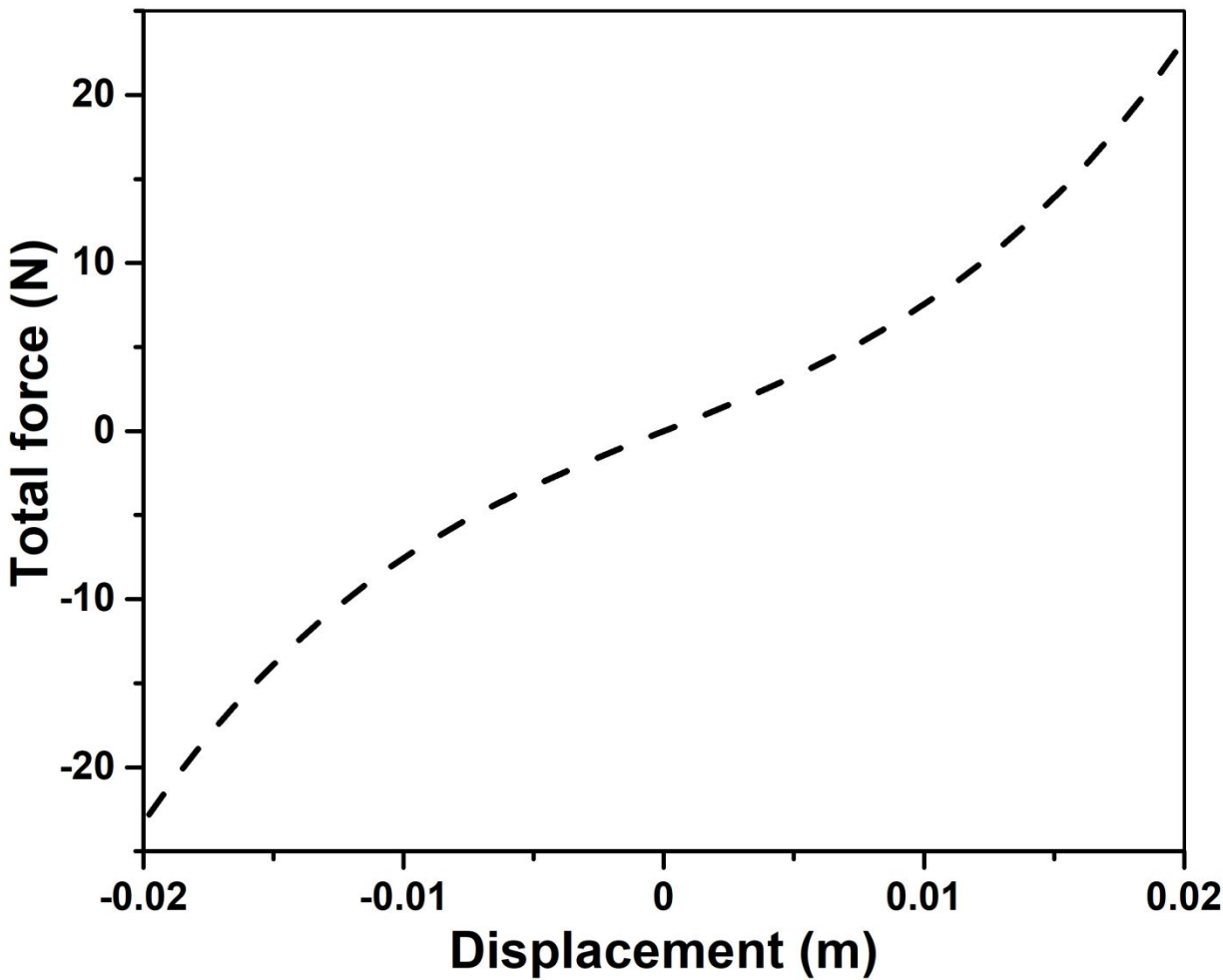
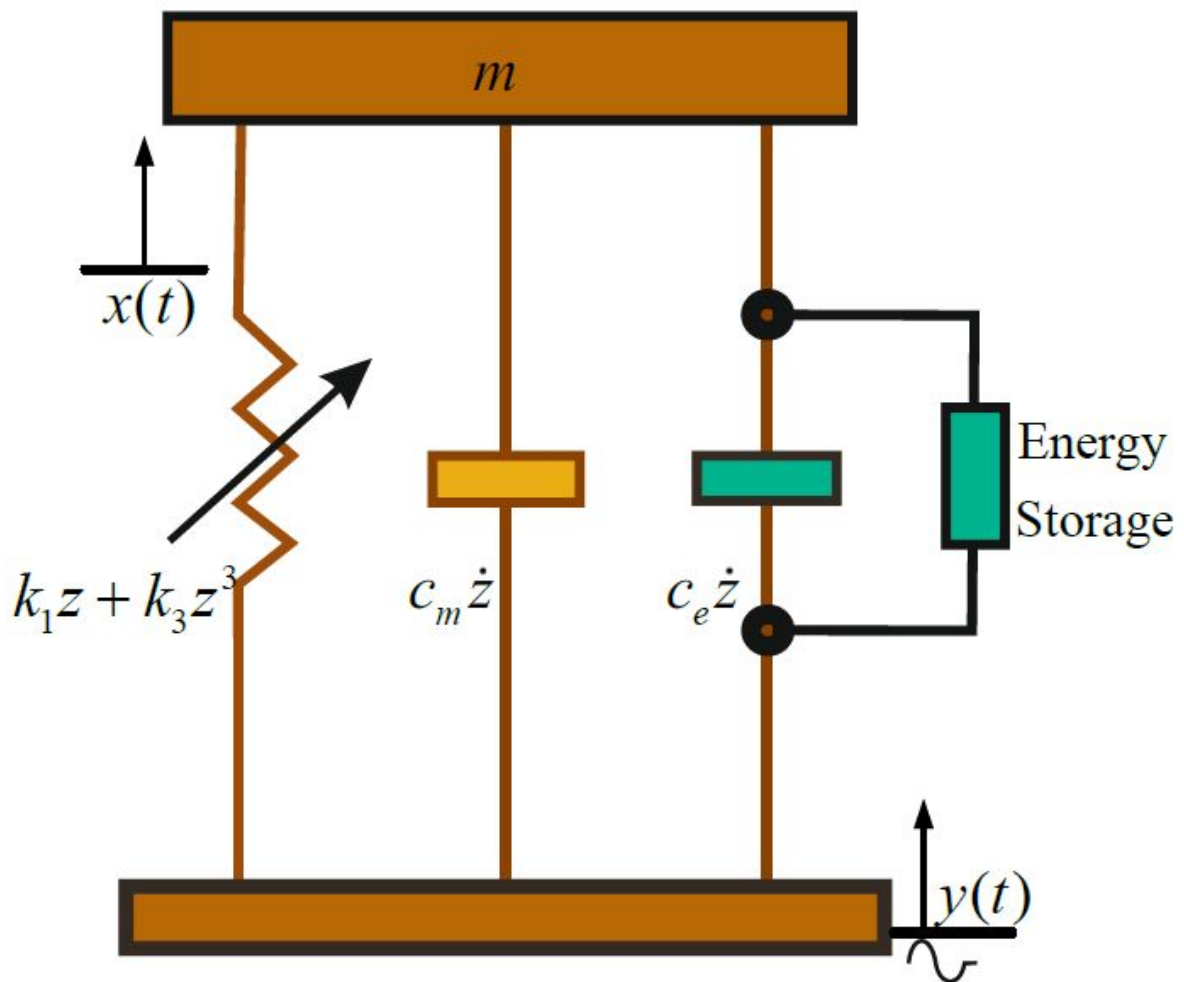
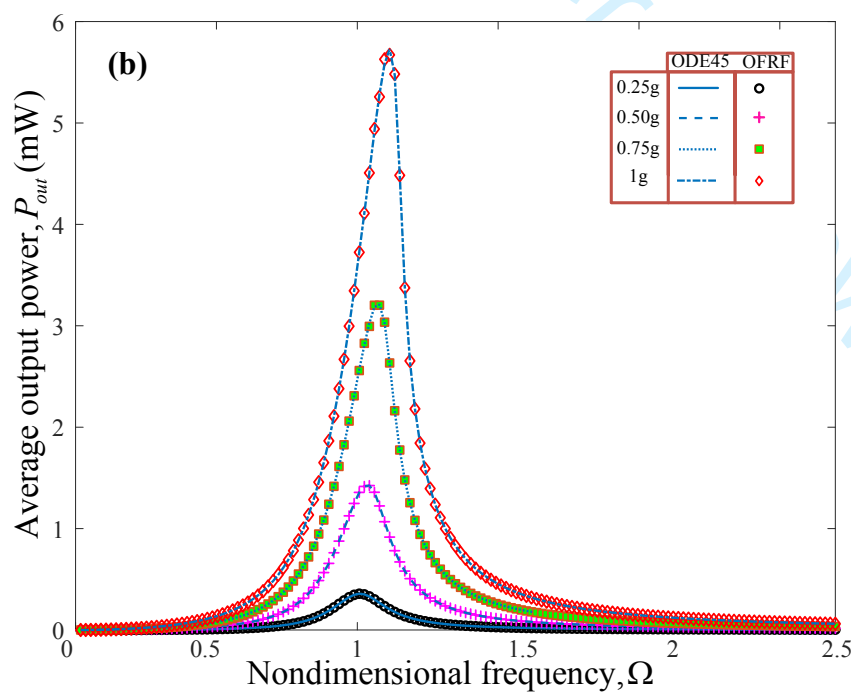
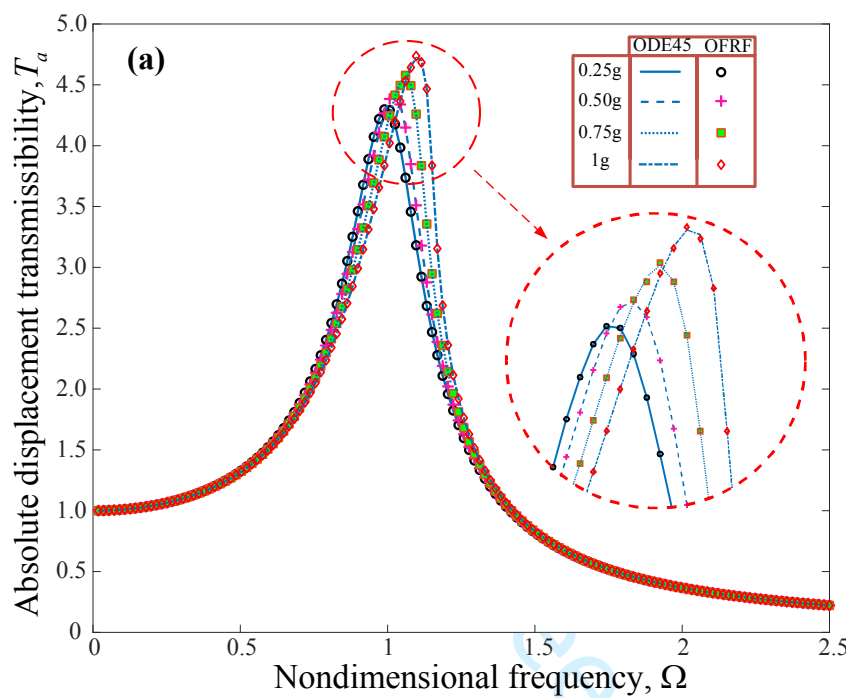


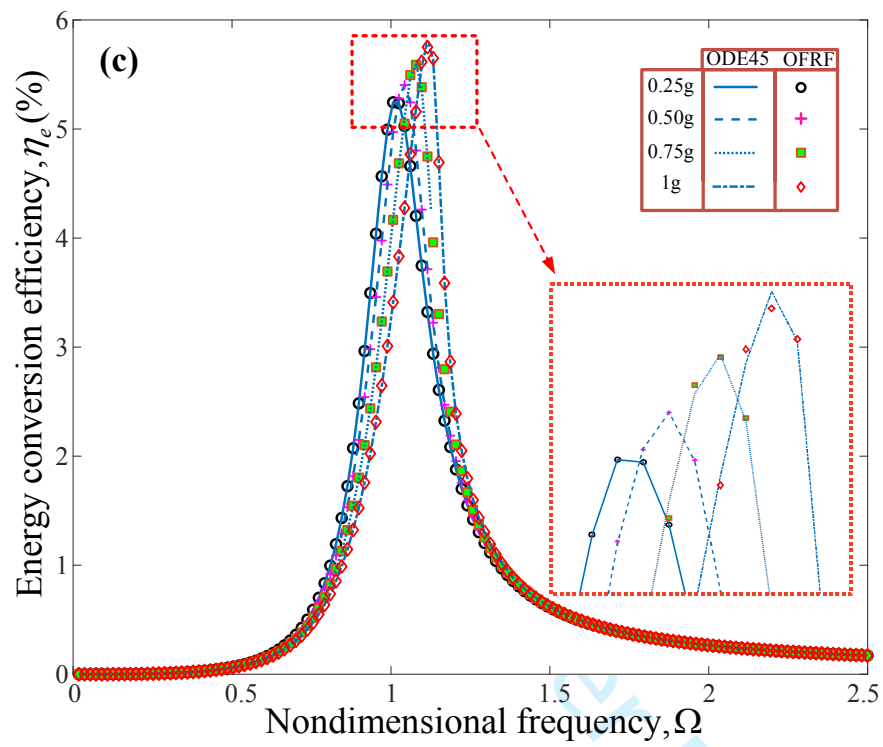
Figure 3: Measured total restoring force of the VI-EH device.



**Figure 4:** Model schematic of the VI-EH device.

1  
2  
3  
4  
5  
6  
7  
8  
9  
10  
11  
12  
13  
14  
15  
16  
17  
18  
19  
20  
21  
22  
23  
24  
25  
26  
27  
28  
29  
30  
31  
32  
33  
34  
35  
36  
37  
38  
39  
40  
41  
42  
43  
44  
45  
46  
47  
48  
49  
50  
51  
52  
53  
54  
55  
56  
57  
58  
59  
60





33 **Figure 5:** Comparison between OFRF analytical and Runge-Kutta numerical solution:  
 34 a) Transmissibility, b) Output power, and c) Energy conversion efficiency at four  
 35 acceleration levels 0.25g, 0.50g, 0.75g, and 1.0g [m.s<sup>-2</sup>].  
 36  
 37  
 38  
 39  
 40  
 41  
 42  
 43  
 44  
 45  
 46  
 47  
 48  
 49  
 50  
 51  
 52  
 53  
 54  
 55  
 56  
 57  
 58  
 59  
 60

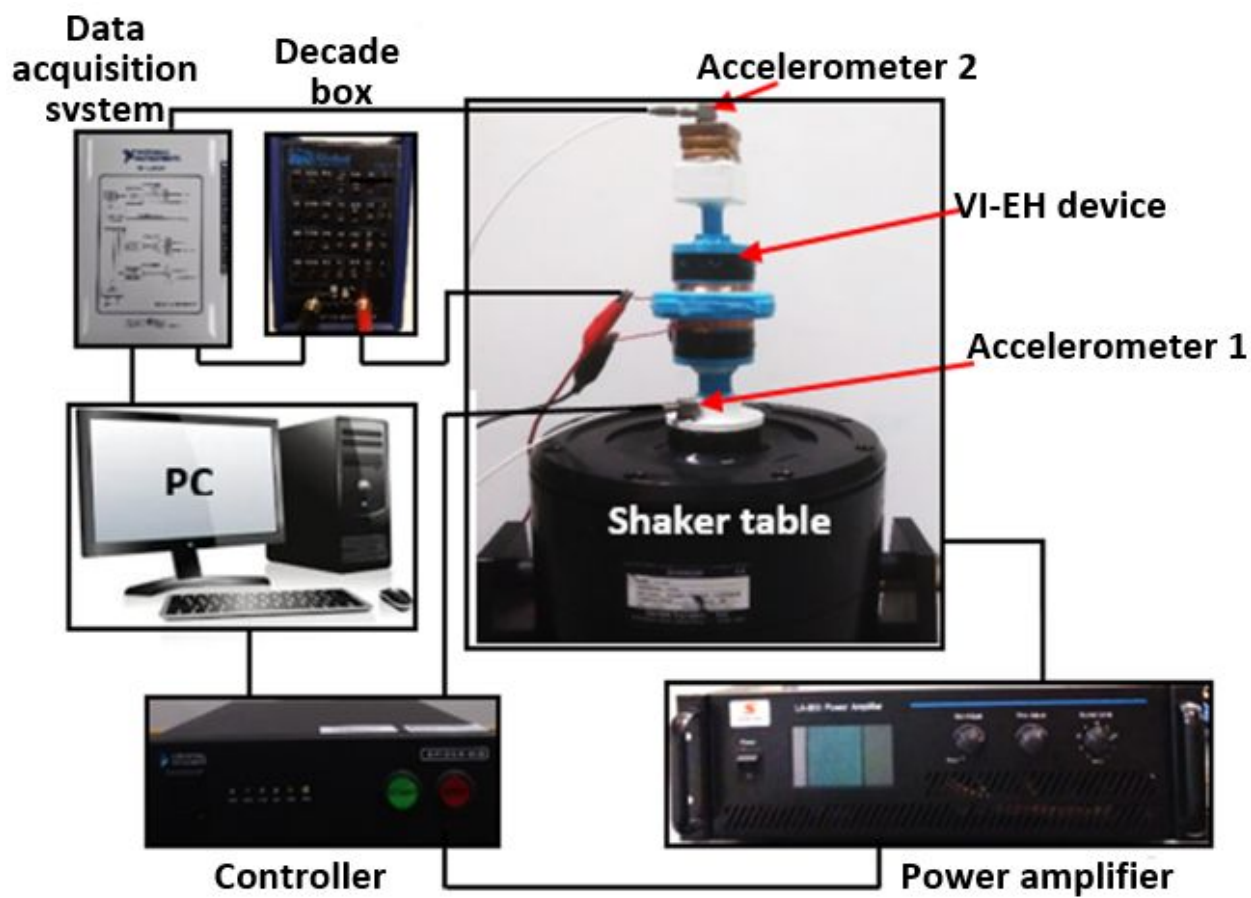
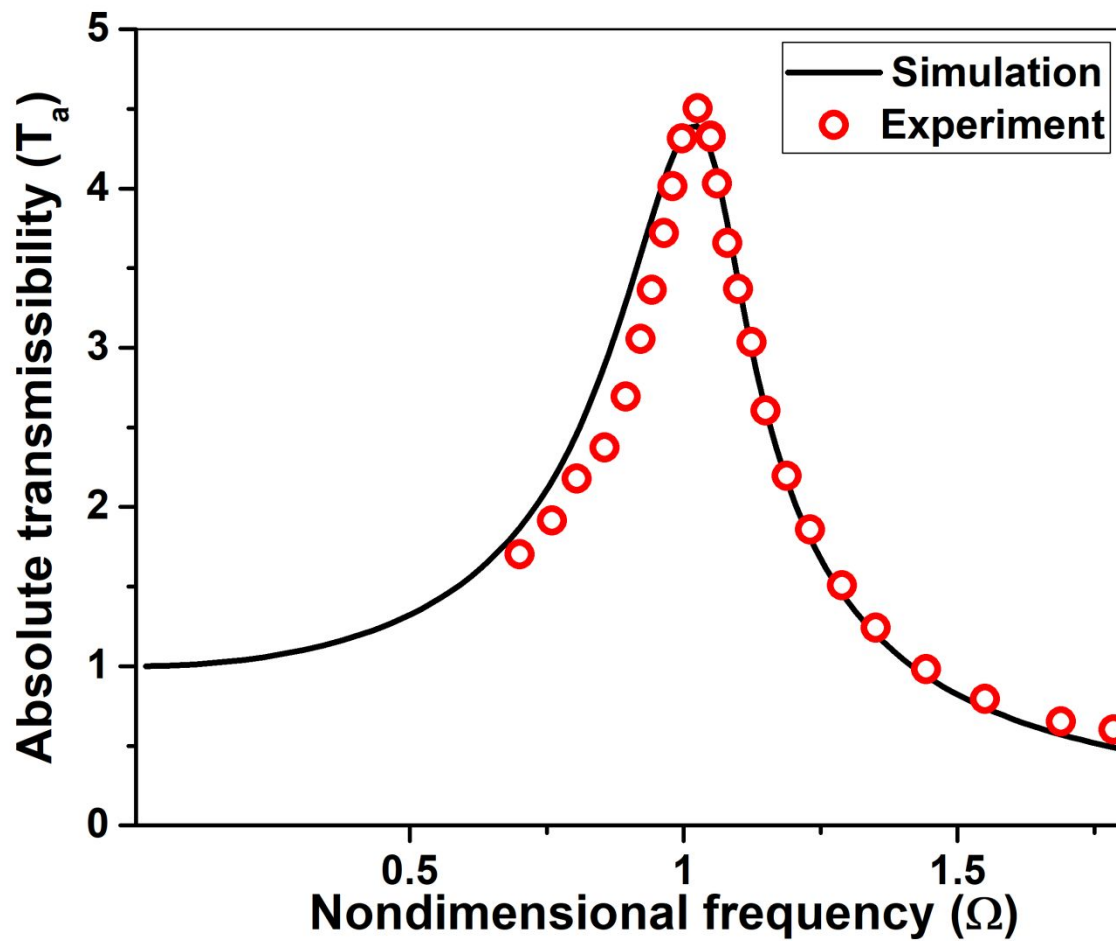


Figure 6: Apparatus used for dynamic characterization of the VI-EH device.



**Figure 7:** Displacement transmissibility of the VI-EH device obtained using both experiment and model at  $0.5g [m.s^{-2}]$ .

1  
2  
3  
4  
5  
6  
7  
8  
9  
10  
11  
12  
13  
14  
15  
16  
17  
18  
19  
20  
21  
22  
23  
24  
25  
26  
27  
28  
29  
30  
31  
32  
33  
34  
35  
36  
37  
38  
39  
40  
41  
42  
43  
44  
45  
46  
47  
48  
49  
50  
51  
52  
53  
54  
55  
56  
57  
58  
59  
60

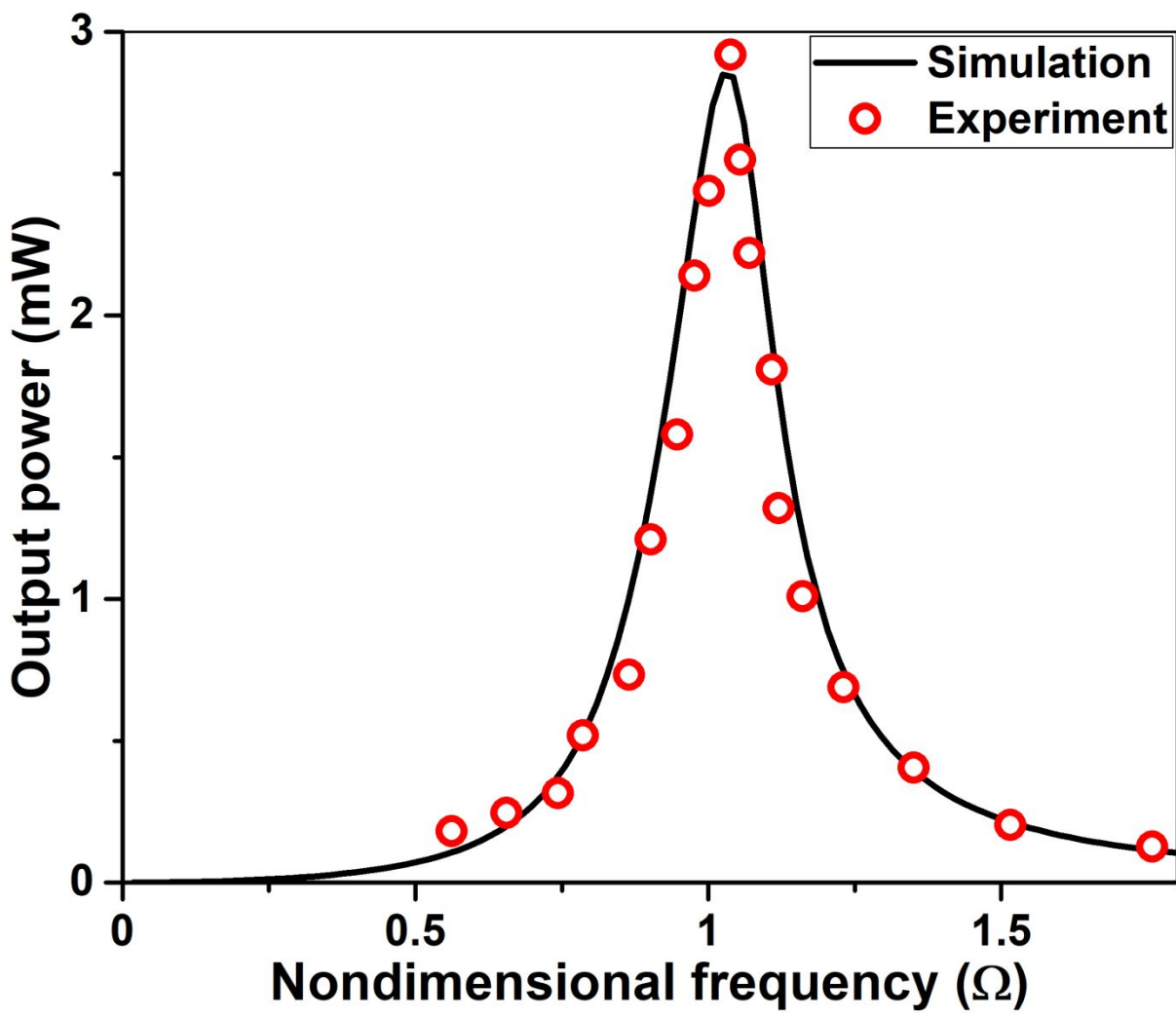
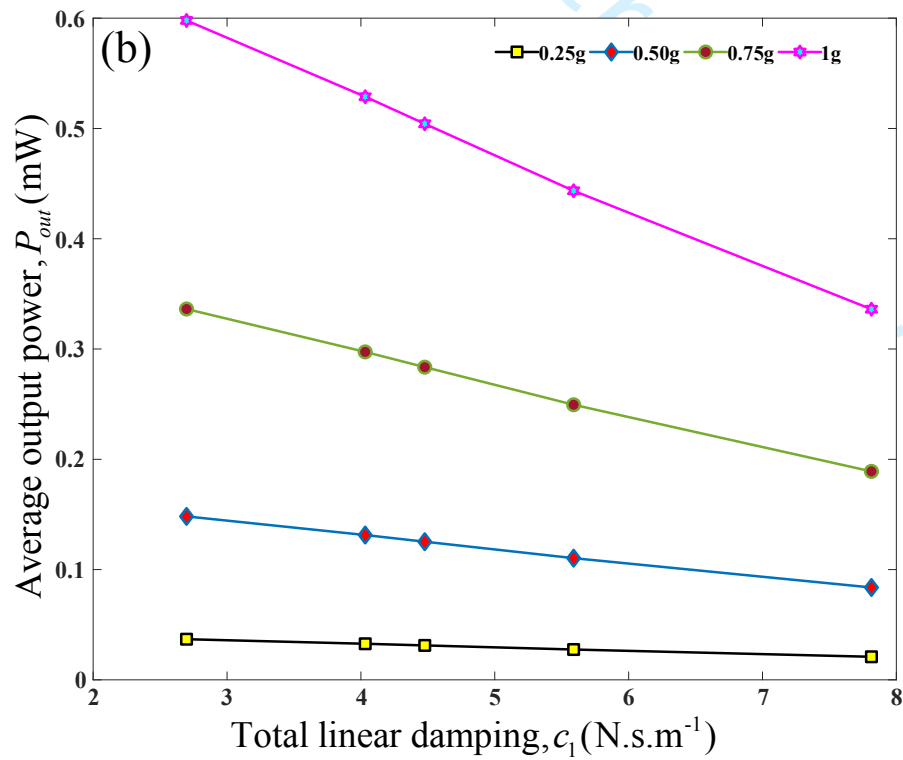
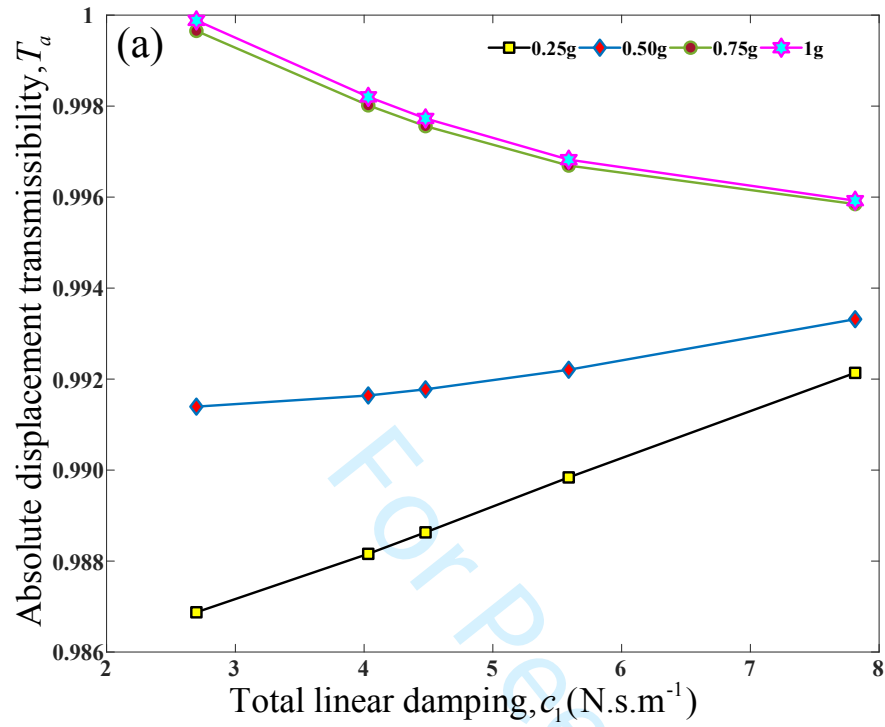
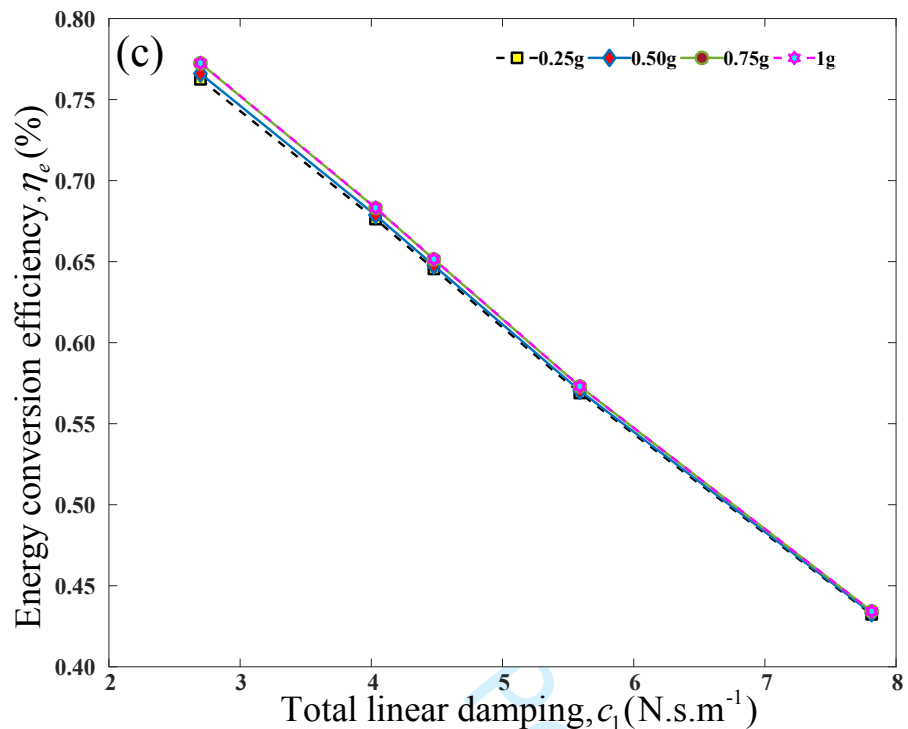
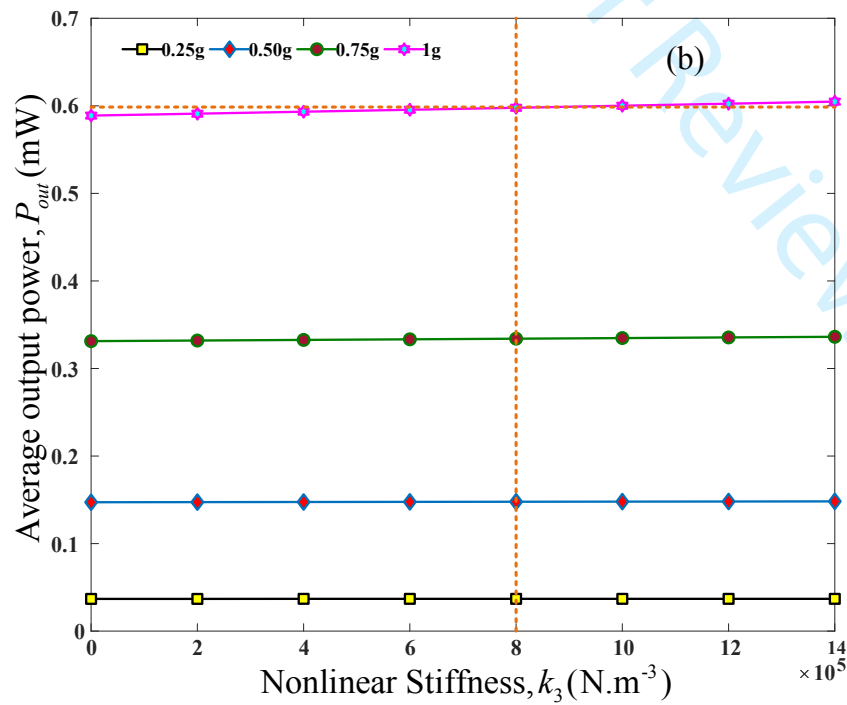
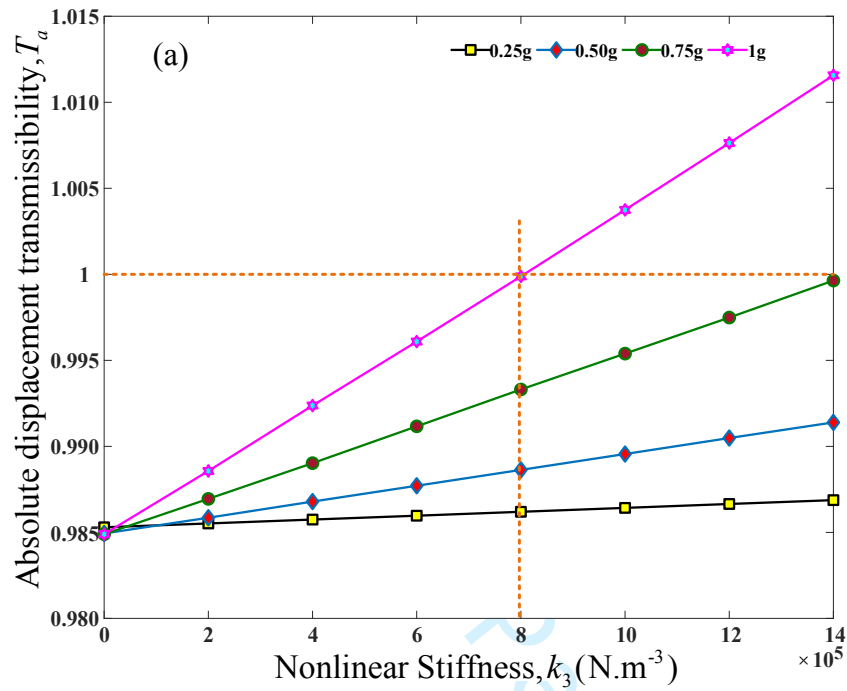


Figure 8: Output power from the VI-EH device obtained using both experiment and model at 0.5g [m.s<sup>-2</sup>].





**Figure 9:** Model simulation of the performance of the VI-EH device subject to variation in linear damping,  $c_1$  while keeping  $k_3$  fixed: a) Transmissibility, b) Output power, and c) Energy conversion efficiency at four acceleration levels 0.25g, 0.50g, 0.75g, and 1.0g [m.s<sup>-2</sup>].



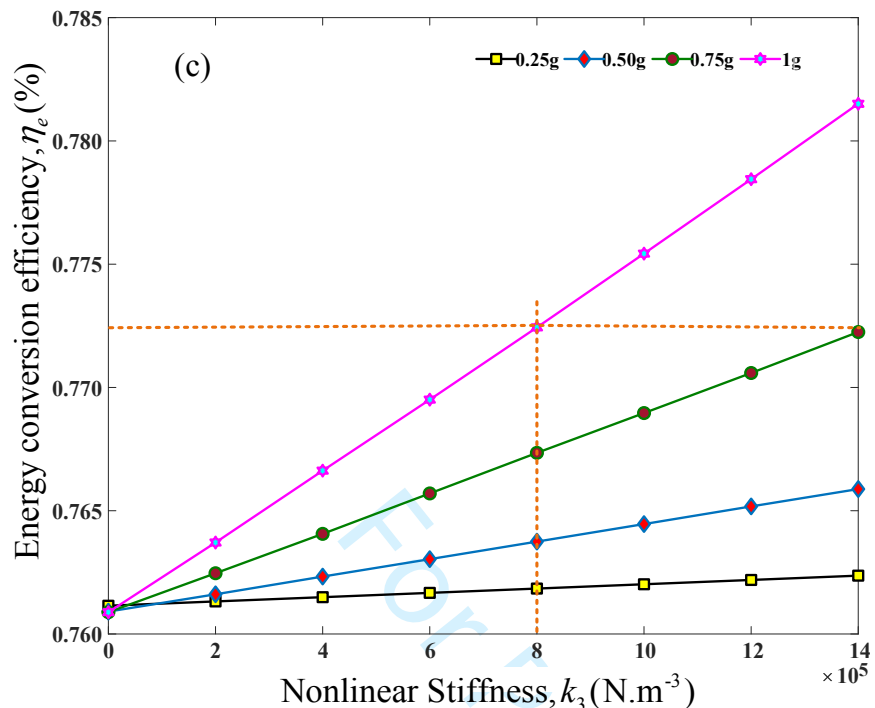


**Figure 10:** Design criteria for the nonlinear stiffness coefficient,  $k_3$  : a) Transmissibility, b) Output power, and c) Energy conversion efficiency at four acceleration levels 0.25g, 0.50g, 0.75g, and 1.0g [m.s<sup>-2</sup>].

**Table I.** Measured systems parameters and properties of the fabricated VI-EH device.

| Parameter                         | Properties                        |
|-----------------------------------|-----------------------------------|
| Coil resistance ( $R_C$ ) [Ohms]  | 1280                              |
| Load resistance ( $R_L$ ) [Ohms]  | 1280                              |
| Coil turns                        | 2000                              |
| Coil material                     | Copper, 40 AWG                    |
| Isolated mass (kg)                | 0.2                               |
| Mechanical spring material        | Thermoplastic poly-Urethane (TPU) |
| $k_3$ [N m <sup>-3</sup> ]        | 1.368e+06                         |
| $k_1$ [N m <sup>-1</sup> ]        | 618                               |
| $c_1$ [N s m <sup>-1</sup> ]      | 2.7                               |
| $\omega_n$ [rad s <sup>-1</sup> ] | 55.61                             |
| B [T]                             | 0.0286                            |

**Table II:** Maximum energy conversion efficiency attainable at  $\omega = 79 \text{ rad s}^{-1}$  ( $W = 1.42$ ) subject to the system constraints at predetermined base accelerations.

| Base acceleration Level [ $\text{m.s}^{-2}$ ] | Absolute displacement transmissibility, $T_a$ | Max. Energy conversion efficiency, $\eta_{e_{\max}}$ (%) | Average output power, $P_{out}$ (mW) | Nonlinear stiffness, $k_3$ ( $\text{N m}^{-3}$ ) |
|---|---|--|--------------------------------------|--|
| 0.25g   | 0.9869  | 0.7624   | 0.037                                | $1.4 \times 10^6$                                |
| 0.50g   | 0.9914  | 0.7659   | 0.148                                | $1.4 \times 10^6$                                |
| 0.75g   | 0.9996  | 0.7723   | 0.336                                | $1.4 \times 10^6$                                |
| 1.00g   | 0.9999  | 0.7724   | 0.598                                | $0.8 \times 10^6$                                |

**Table III:** Maximum energy conversion efficiency attainable at specific nonlinear stiffness value subject to the system constraints considering the normalized weight contribution of each excitation.

| Set of normalized weight contributions | Absolute displacement transmissibility, $T_a^K$ | Max. Energy conversion efficiency, $\eta_{e_{max}}^K$ (%) | Average output power, $P_{out}^K$ (mW) | Nonlinear stiffness, $k_3$ (N m <sup>-3</sup> ) |
|--|---|---|--|---|
| $k_1 = k_2 = k_3 = k_4 = 0.25$         | 0.9974  | 0.7705  | 0.282                                  | $1.4 \times 10^6$                               |
| $k_1 = k_2 = 0.5, k_3 = k_4 = 0$       | 0.9891  | 0.7641  | 0.0925                                 | $1.4 \times 10^6$                               |
| $k_1 = k_2 = 0, k_3 = k_4 = 0.5$       | 0.9996  | 0.7722  | 0.471                                  | $1 \times 10^6$                                 |